Theoretical predictions and experimental measurements of sound transmission through a flat plate and a cylindrical shell

by

Fatima Ezzahra Taha

A thesis submitted to the Graduate Faculty of
Auburn University
in partial fulfillment of the
requirements for the Degree of
Master of Science

Auburn, Alabama
August 5, 2017

engineering, mechanical, acoustics, sound, transmission, intensity

Approved by

Malcolm Crocker, Chair, Professor Emeritus, Department of Mechanical Engineering
George Flowers, Professor and Dean of Graduate School, Department of Mechanical Engineering
Subhash Sinha, Professor Emeritus, Department of Mechanical Engineerin

Abstract

Sound transmission through a flat plate and a cylindrical shell was studied both theoretically and experimentally. The theory consisted of using statistical energy analysis (SEA) to predict the transmission loss of each structure. The experimental part included the use of sound pressure levels obtained using microphones and of sound intensity using a sound intensity probe to calculate sound transmission loss. Results, both theoretical and experimental, were then compared to draw conclusions concerning the best way to measure sound transmission through structures and how reliable the theory is, the behavior of structures made of the same material but of different shapes was also of concern in this study.

Acknowledgments

I would first like to thank my thesis advisor Dr Malcolm Crocker of the mechanical engineering departments at Auburn University. The door to Dr Crocker's office was always open whenever I faced a problem or had a question about my research or writing. He consistently allowed this thesis to be my own work but guided me whenever I needed it. In addition, I would like to express my gratitude to Professors Georges Flowers and Subhash Sinha who served on the faculty advisory committee.

I would also like to acknowledge Pouria Oliazadeh and Margarita Maksotskaya for their valuable help during the completion of this thesis.

Finally, I must express my very profound gratitude to my parents for providing me with unfailing support and continuous encouragement throughout my years of study and through the process of researching and writing this thesis. This accomplishment would not have been possible without them. Thank you.

Fatima Ezzahra Taha

Table of Contents

List of Figures

List of Symbols

A_p	panel surface area
c_0	speed of sound in air
D	flexural rigidity
E	Young's modulus
E_i	total energy of subsystem *i*
f	frequency
f_c	critical coincidence frequency
f_r	ring frequency
h	panel thickness
I_{in}	incident sound intensity level
I_{out}	transmitted sound intensity level
k_a	cylinder longitudinal wavenumber
k_c	cylinder transversal wavenumber
L	cylinder length
l_1	panel length
l_2	panel width
λ_a	acoustic wavelength
λ_c	critical coincidence wavelength
m	longitudinal mode number
m_s	panel mass surface per unit area
M_p	panel mass
N	number of modes

n	transverse mode number
N.R.	noise reduction
η_{rad}	panel radiation efficiency
η_{int}	internal loss factor
η_m	roots of the beam equation
η_{ij}	coupling loss factor between system *i* and system *j*
n_i	modal density of subsystem *i*
η_i	internal loss factor of subsystem *i*
P	panel perimeter
P_{in}	incident sound pressure level
P_{out}	transmitted sound pressure level
P_r	radiated pressure
Π_{in1}	power supplied to subsystem *i*
Π_{ij}	rate of energy flow from subsystem *i* to subsystem *j*
Π_{dissi}	rate of internal energy dissipation on subsystem *i*
ρ_0	density of air
ρ_m	density of material
$R_{rad}^{2\pi}$	panel radiation
R	cylinder radius
R_{mech}	mechanical resistance
S	cylinder surface area
S_a	spectral density of panel acceleration
S_{aml}	spectral density of panel acceleration predicted by mass law
S_{p1}	spectral density of pressure in transmission room
$\boldsymbol{\sigma}$	radiation efficiency

T.L.	random incidence transmission loss
TL	transmission loss
TL_{res}	resonant transmission loss
TL_{nr}	nonresonant transmission loss
T_R	reverberation time
U_x	displacement of the cylinder in the longitudinal direction
U_θ	displacement of the cylinder in the circumferential direction
U_z	displacement of the cylinder in the transverse direction
μ	Poisson's ratio
V_i	volume of room i
v	velocity of the radiating surface
v_0	normalized frequency
ω	angular frequency
ω_0	normalized angular frequency
ω_{mn}	natural angular frequency

Chapter 1: Introduction

Flat plates (panels) and cylindrical shells are very commonly used structures in engineering and other fields. Panels are mostly found in solar collectors or used as aircraft panels, whereas cylindrical shells are found in many practical devices such as air-conditioning ducts and aircraft cabins. Thus, studying the properties of these structures in terms of sound transmission has become an important and useful step in developing better equipment or improving the existing structures [1].

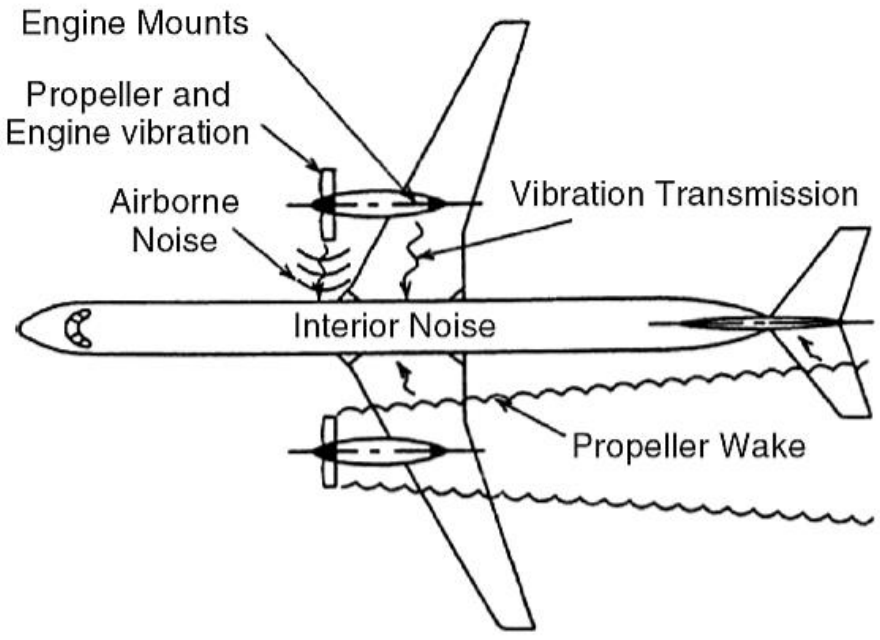

Figure 1: Example of a system using a cylindrical shell [1].

One of the most important properties of a structure is its sound reduction index commonly called transmission loss. Transmission loss is related to the decrease in sound intensity experienced as a sound pressure wave propagates through a structure. Understanding of this characteristic can be very helpful in reducing interior noise levels for instance in aircraft cabins. In this regard, the development of accurate prediction approaches and experimental measurement methods is very important in the study of noise propagation through structures.

Different theoretical approaches to study structural properties in sound transmission exist, the most commonly used are the Statistical Energy Analysis and the Finite Elements Method. The Finite Elements Method is a very popular numerical method based on a partial differential equation formulation of a problem and is useful when studying the behavior of a structure on a large scale [2, 3]. Statistical Energy Analysis however, is better suited to the study of complex structures even though the results at low frequencies are not considered very reliable. Statistical Energy Analysis was implemented in the late 1950s independently by Richard Lyon and Preston Smith [4, 5, 6] for linearly coupled oscillators and by Crocker, Price and Bhattacharya [7, 8] for transmission of sound through structures, with the aim of analyzing the response of large complex aerospace structures subjected to random loading. For the panel and the cylindrical shell studied in this thesis, the critical frequency was high which made the use of Statistical Energy Analysis applicable. Chapter 2 of this thesis reviews the theoretical aspect of Statistical Energy Analysis and how it can be applied to each of the structures under consideration. It also describes the computation used to obtain the so-called transmission loss for each structure.

"Mass law theories' [9, 10] were used prior to Statistical Energy Analysis to predict sound transmission loss, however their limitations were known since they do not take into account the stiffness and damping of the structures. "Mass law theories" are also briefly discussed in Chapter 2.

Different experimental approaches exist to measure sound transmission loss of panels and shells. The first approach consists of using sound pressure level measurements made each side of the panel or shell to calculate the noise reduction created by the structure. Then applying a formula obtained from theory to calculate transmission loss. It is also called the transmission suite method or the two room method [11]. A second approach consists of using sound intensity measurements [12, 13] to determine the transmission loss by calculating the sound intensity incident on the structure and measuring the transmitted sound intensity using a sound intensity probe. Chapter 3 presents the setup used for each structure and each method used as well as the results obtained with both methods for each structure. Chapter 4 compares the results obtained using the theoretical approach and the experimental ones and presents conclusions concerning which experimental method provides the most reliable results. This chapter also focuses on a comparison of the acoustical behaviors of the two structures and on forming conclusions concerning the differences found between the two structures. Finally, Chapter 5 discusses general conclusions of this study.

Chapter 2: Statistical Energy Analysis theory

2.1-Overview:

A theory that explains sound transmission through a complex structure is referred to as Statistical Energy Analysis (SEA). It has been studied by several scientists and constitutes a very important part of acoustics. The analytical model study was conducted using this method which aims to predict the vibrations in a system at high frequency where it is difficult to apply the finite element method. Transmission Loss was the most important parameter in this study.

SEA consists of subdividing the system under study into coupled subsystems and analyzing the energy flow in these subsystems under the assumption that the energy flow between coupled systems is proportional to the modal energy difference between the systems. An assumption is made that the coupling is weak and linear, as is the case for the subsystems in this study [14].

Since the calculations used in SEA are in frequency bands (one-octave or one-third octave), the results are averages in frequency bands. Energy is the main variable used in this method in which the system is divided into subsystems. The average energy levels of each subsystem are converted into the needed variables (sound pressure levels etc.). Lyon has emphasized the fact that SEA is not a specific technique, but a set of tools [14]. Many scientists have used the SEA model to measure transmission loss of different structures; the aim of the theoretical part of this study is to adapt this method to the two structures under study.

2.2-Application of SEA to the study of the flat panel

2.2.1-Critical frequency and modes of the panel:

The critical frequency of the panel occurs when the panel bending wavelength equals the trace wavelength of grazing sound waves and can easily be calculated using the formula: $f_c = \sqrt{\frac{3\rho_m}{E}}\frac{c_0^2}{\pi h}$ where ρ_m is the mass density of the material, E is Young's modulus, c_0 is the speed of sound in air and h is the thickness of the structure [15].

The vibration of panels is higher at the critical frequency; therefore the transmission of sound is also higher. To study the vibration of the panel below and above the critical frequency, it is necessary to study the resonant modes of the panel.

The resonant modes of a panel can be classified into two categories: Acoustically fast modes and acoustically slow modes. The modal behavior of a panel is different in each of these categories.

Acoustically fast modes are modes that have structural bending wave speeds greater than the speed of sound in air and are above the critical frequency. These modes have high radiation efficiencies. Acoustically slow modes have resonance frequencies below the critical frequency and bending wave speeds less than the speed of sound. Acoustically slow modes have low radiation efficiencies and can be subdivided into two classes: edge modes and corner modes. With edge modes, the bending phase speeds in one direction are greater than the speed of sound

whereas in the other direction they are smaller. With corner modes, both bending phase speeds in both directions are less than the speed of sound.

Below the critical frequency, where acoustically slow modes are resonant, trace matching does not exist at resonance, the vibration amplitude is low and most sound is transmitted by modes that are non-resonant. This gives rise to the so-called "mass-law" transmission. Above critical frequency, trace matching occurs and the vibration amplitude of the panel is high, then sound transmission is mostly resonant. Then as the frequency increases, the sound transmission approaches "mass law" predictions again.

2.2.2- Radiation of the panel:

The radiation resistance of a structure is a measure of the coupling of the structure with the acoustic field, or a measure of the sound power radiated by the structure for a vibration level. Determining the radiation resistance of the panel is important in further determinations of the transmission loss. The radiation resistance of a simply-supported panel to half space is given by Maidanik [16, 17] by the formula:

$$R_{rad}^{2\pi} = A_p \rho_m c_0 . \begin{cases} \left(\lambda_c \lambda_a / A_p\right) 2(f/f_c) g_1(f/f_c) + \left(P \lambda_c / A_p\right) g_2(f/f_c), & f < f_c; \\ (l_1/\lambda_c)^{-1/2} + (l_2/\lambda_c)^{1/2}, & f = f_c; \\ (1 - f_c/f)^{-1/2}, & f > f_c, \end{cases}; \qquad (1)$$

where:

$$g_1(f/f_c) = \begin{cases} (4/\pi^4)(1 - 2\alpha^2)/\alpha\,(1 - \alpha^2)^{1/2}, & f < \frac{1}{2} f_c, \\ 0, & f > \frac{1}{2} f_c, \end{cases};$$

$$g_2(f/f_c) = (2\pi)^{-2} \{(1 - \alpha^2) \ln[(1 + \alpha)/(1 - \alpha)] + 2\alpha\}/(1 - \alpha^2)^{3/2}\,,\ \alpha = (f/f_c)^{1/2}.$$

Here, A_p is the area of the panel, P is the perimeter of the panel, λ_c is the coincidence wavelength of the panel, and λ_a is the acoustic wavelength.

Then, the radiation loss factor of the panel can be defined as:

$$\eta_{rad} = \frac{R_{rad}^{2\pi}}{\omega M_p} \; ; \tag{2}$$

where ω is the angular frequency and M_p is the mass of the panel.

The response of the panel to acoustic excitation depends on the radiation resistance and the radiation loss factor of the panel.

2.2.3-Panel response and sound transmission Loss:

To determine the transmission loss, the system is subdivided into three coupled subsystems and energy flow through these systems is studied in frequency bandwidths of 1 rad/sec as described by Crocker and Price [16]:

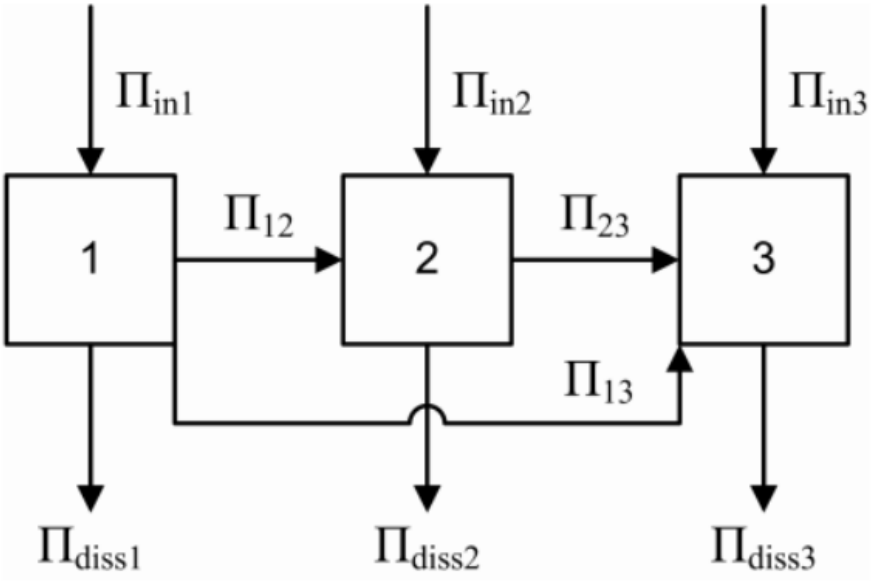

Figure 2: Energy flows between subsystems [4, 16].

The first subsystem (1) represents the source room where the noise source is located, the second subsystem (2) is the panel itself, clamped between the two rooms and the third system (3) is the receiving room. The following figure, Figure 3 is a representation of the system:

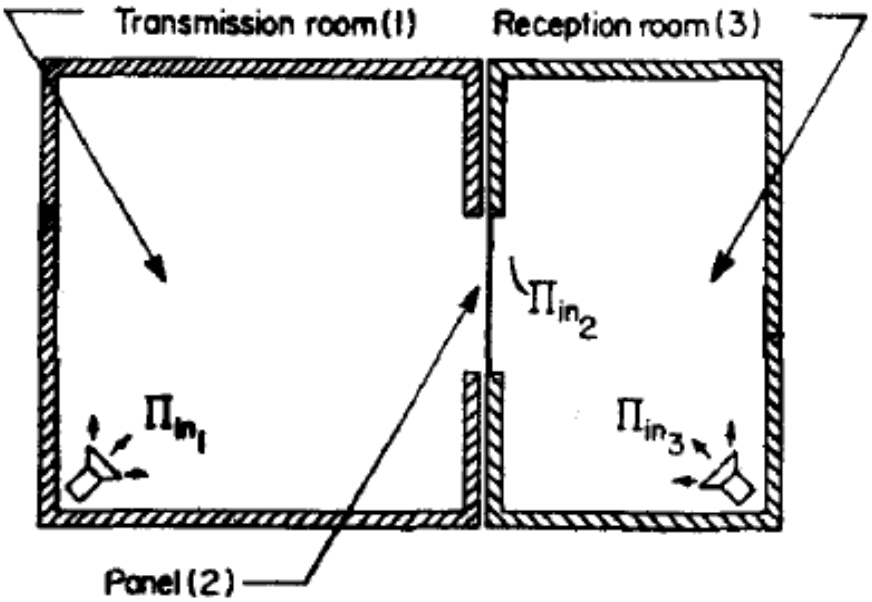

Figure 3: Setup of the panel clamped between two reverberant rooms. [18]

In the following equations, Π_{in1} is the power supplied to system *i*, Π_{ij} is the rate of energy flow from system *i* to system *j*, Π_{dissi} is the rate of internal energy dissipation in system *i*, E_i is the total energy of system *i*, n_i is the modal density of system *i* in radian frequency, η_{ij} is the coupling loss factor between system *i* and system *j*, η_i is the internal loss factor of system *i*. The power flow balance between the three subsystems can be written as follows:

$$\Pi_{in1} = \Pi_{diss1} + \Pi_{12} + \Pi_{13} \; ; \tag{3}$$

$$\Pi_{in1} = \omega\eta_1 E_1 + \omega\eta_{12} n_1 \left(\frac{E_1}{n_1} - \frac{E_2}{n_2}\right) + \omega\eta_{13} n_1 \left(\frac{E_1}{n_1} - \frac{E_3}{n_3}\right) ; \tag{4}$$

$$\Pi_{in2} = \Pi_{diss2} - \Pi_{12} + \Pi_{23} \; ; \tag{5}$$

$$\Pi_{in2} = \omega\eta_2 E_2 - \omega\eta_{12} n_1 \left(\frac{E_1}{n_1} - \frac{E_2}{n_2}\right) + \omega\eta_{23} n_2 \left(\frac{E_2}{n_2} - \frac{E_3}{n_3}\right) \quad ; \tag{6}$$

$$\Pi_{in3} = \Pi_{diss3} - \Pi_{13} - \Pi_{23}; \tag{7}$$

$$\Pi_{in3} = \omega\eta_3 E_3 - \omega\eta_{13} n_1 \left(\frac{E_1}{n_1} - \frac{E_3}{n_3}\right) - \omega\eta_{23} n_2 \left(\frac{E_2}{n_2} - \frac{E_3}{n_3}\right); \tag{8}$$

For this model, reverberant sound is produced by a loudspeaker, therefore $\Pi_{in2} = \Pi_{in3} = 0$ and by substitution into the above equations:

$$\frac{E_2}{n_2} = \frac{E_1}{n_1}\left[\frac{\eta_{rad}}{\eta_{int}+2\eta_{rad}}\right]; \tag{9}$$

$$E_3 = \frac{E_1\eta_{13}+E_2\eta_{23}}{\eta_3+\eta_{31}+\eta_{32}}. \tag{10}$$

Then, noise reduction from the source room to the receiving room is given by the equation:

$$\frac{E_3}{E_1} = \frac{\eta_{13}+\eta_{rad}^2(n_2/n_1)/(\eta_{int}+2\eta_{rad})}{\eta_3+(n_1/n_3)\eta_{13}+(n_2/n_3)\eta_{rad}}; \tag{11}$$

η_{rad} was determined by Equation (2) and $\eta_{13}$is determined by the equation:

$$10\log_{10}\eta_{13} = -\text{T.L.} + 10\log_{10}\left(\frac{A_p c_0}{4V_1\omega}\right); \tag{12}$$

where T.L. is the random incidence mass law transmission loss value for the panel which is given by the equation: T.L.=$10\log[\frac{\omega^2 M_p^2}{4\rho_0^2 c_0^2}]$.

Finally, $\eta_3 = \frac{2.2}{fT_R}$, where $T_R$is the reverberation time of the receiving room.

The noise reduction of the panel is determined by taking the logarithm of Equation (11):

$$\text{N.R.} = 10\log_{10}[\eta_{13} + \eta_{rad}^2(n_2/n_1)/(\eta_{int} + 2\eta_{rad})] - 10\log_{10}[\eta_3 + (n_1/n_3)\eta_{13} + (n_2/n_3)\eta_{rad}]. \tag{13}$$

The room modal densities at high frequency are assumed to be:

$$\left.\begin{aligned} n_1 &= \frac{V_1\omega^2}{2\pi^2 c_0^3} \\ n_3 &= \frac{V_3\omega^2}{2\pi^2 c_0^3} \end{aligned}\right\}. \tag{14}$$

where V_i is the volume of room *i*.

Finally, the transmission loss is found using the formula:

$$\mathrm{TL} = \mathrm{N.R.} + 10\log_{10}\left[\frac{A_p c_0 T_R}{24 V_3 \ln(10)}\right]. \tag{15}$$

2.2.4-Panel response relative to mass law theory:

Equation (9) gives the panel vibration amplitude. As stated by Crocker [16, 18] or a reverberant field, the total energy in a 1 rad/sec frequency bandwidth is $E_1 = \frac{S_{p1}V_1}{\rho_0 c_0^2}$ and the total panel energy in 1 rad/sec frequency bandwidth is: $\mathrm{E}_2 = \frac{\mathrm{M_p S_a}}{\omega^2}$ and Equation (9) becomes:

$$\frac{M_p S_a}{n_2 \omega^2} = \frac{S_{p1}V_1}{\rho_0 c_0^2 n_1}\left[\frac{\eta_{rad}}{\eta_{int}+2\eta_{rad}}\right]; \tag{16}$$

Using the modal density of the room, n_1, and the modal density of the panel, n_2, given by Equation (15)

$$\frac{S_a}{S_{p1}} = \frac{\pi^2 f_c}{\rho_0 c_0 \rho_m h}\left[\frac{\eta_{rad}}{\eta_{int}+2\eta_{rad}}\right]; \tag{17}$$

If the panel responded as a limp mass, the response would be:

$$\frac{S_{aml}}{S_{p1}} = \frac{2}{(\rho_m h)^2}; \tag{18}$$

Finally, dividing Equation (17) by Equation (18) gives the panel response relative to mass law:

$$\frac{S_a}{S_{aml}} = \frac{\pi^2 f_c \rho_m h}{\rho_0 c_0} \left[\frac{\eta_{rad}}{\eta_{int}+2\eta_{rad}}\right]. \quad (19)$$

2.2.5-Computational implementation:

Using the equations in the theory above, a program was written to compute the noise reduction and transmission loss at each frequency for the panel as well as the response of the panel relative to mass law. The thin flat panel used in the program has the same values as the panel used for the experimental part for its different parameters. The panel was 1.04 m long, 0.609 m wide and 0.00127 m thick. The material chosen for the panel was galvanized steel metal with an estimated density of 7,850 kg/m^3 , Young's modulus of 200 GPa, and Poisson's ratio of 0.28. The program is given as an appendix.

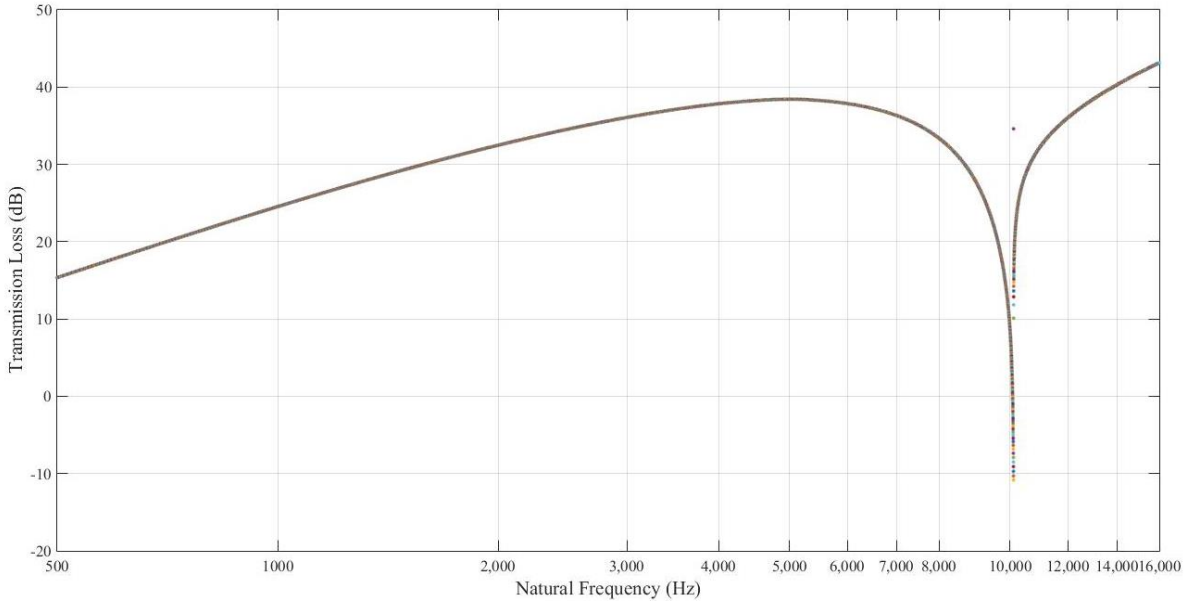

Figure 4: Theoretical transmission loss of the panel using SEA.

The program was run for frequencies ranging from 500 Hz to 16,000 Hz where SEA is the most accurate. At the critical frequency, a significant dip can be seen. The panel becomes transparent to sound. The transmission loss is lower than it is at all the other frequencies and does not follow "mass law" theory which does not take into account the stiffness and the damping of the panel.

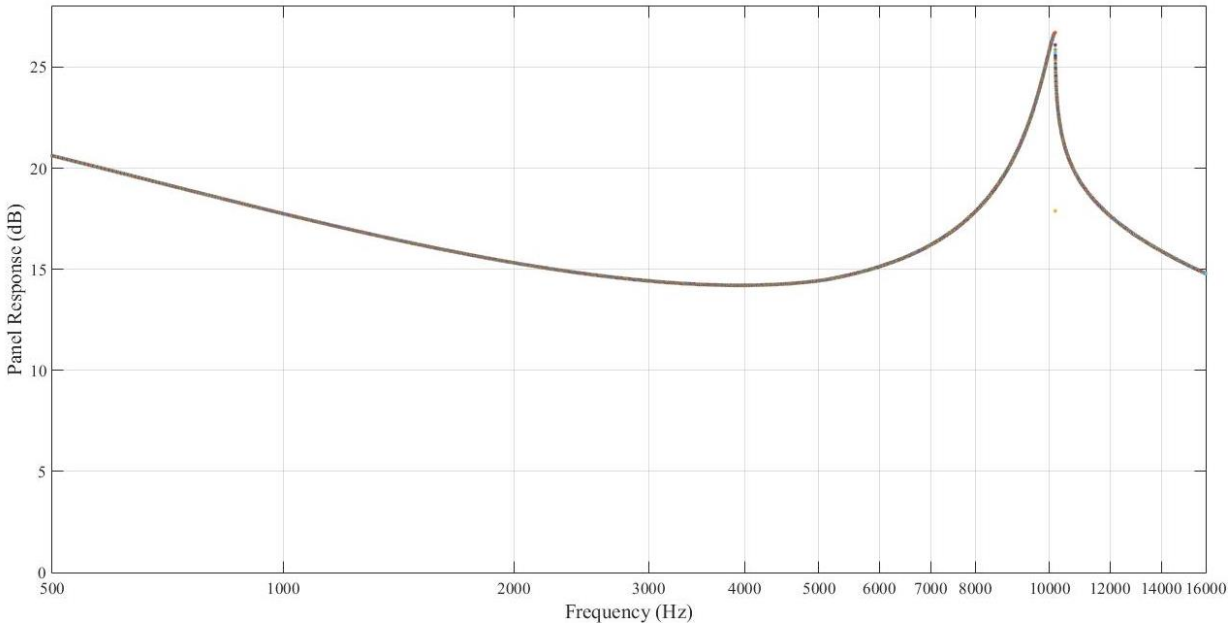

Figure 5: Predicted panel response relative to mass law.

2.3- Application of SEA to the study of the cylinder:

As Lyon explains [14], SEA requires one to determine the parameters that will later be used to calculate the system response. Among these parameters, the most important are the natural frequencies of the cylinder that can be found theoretically, the modal density, the mode classification and loss factors which can be obtained using a powerful approach in SEA known as the wavenumber diagram.

2.3.1-Natural frequencies and modes of the cylinder:

The natural frequencies of a cylindrical shell are obtained using the equation of motion derived from Love's equation [19, 20], for a simply supported cylinder, the displacements in the longitudinal, circumferential and transverse directions, respectively U_x, U_θ and U_z are:

$$\begin{cases} U_x = A\cos(\dfrac{m\pi x}{L})\cos(n(\theta-\varphi)) \\ U_\theta = B\sin(\dfrac{m\pi x}{L})\sin(n(\theta-\varphi)) \\ U_z = C\sin(\dfrac{m\pi x}{L})\cos(n(\theta-\varphi)) \end{cases} ; \quad (20)$$

where θ and *x* are the coordinates, *m* and *n* are the longitudinal and transverse mode numbers and φ is an undetermined angle.

Theoretically, the solution (natural frequencies) can be found by substituting the eigen-functions into the equation of motion. But this solution usually proves to be too complicated to be used in an engineering model [21]. This problem, however, can be solved by only considering the transverse vibration which gives us the Donnell-Mushtari-Vlasov equation [22, 23, 24] by making the following assumptions [25, 26]:

-Neglecting the contribution of in-plane deflection in bending strain expressions.

-Neglecting the influence of inertia in the in-plane direction.

-Neglecting the shear terms in the transverse direction.

-Satisfying the inequality: $\frac{n^2}{R^2} > \frac{\lambda_a}{L^2}$ where R is the radius, L is the length of the cylinder and n is the mode number [25].

Using these simplifications, the natural angular frequencies of the cylinder can be written:

$$\omega_{mn} = \sqrt{\frac{1}{\rho_m h}\frac{EhR^2}{L^4 n^4}\eta_m + D(\frac{n}{R})^4} \quad ; \tag{21}$$

where ρ_m is the mass density of the material, m and n are respectively the mode numbers in the longitudinal and transversal directions, E is Young modulus, D is the bending stiffness, and the η_m values are the roots of the analogous beam equation determined by boundary conditions.

Soedel [27] explained that the last assumption is not necessary for all cases, including the case of a simply-supported cylinder. Without using this simplification, the natural angular frequencies become:

$$\omega_{mn} = \sqrt{\frac{1}{\rho_m h}\left[\frac{Eh\eta_m^4}{R^2 L^4\left[\frac{n^2}{R^2}+\frac{\eta_m^2}{L^2}\right]^2} + D\left[\frac{n^2}{R^2}+\frac{\eta_m^2}{L^2}\right]^2\right]}. \tag{22}$$

The boundary conditions have an influence on the variables in Equation (22). It has been shown, however, that these differences are smaller for higher mode numbers, which means that the error in calculations is only limited to lower modes (m, n <5) when the cylinder is assumed to be simply-supported.

The wavenumber diagram:

The wave-number diagram, also called the *k*-space diagram is a very powerful approach used in the SEA in order to simplify then plot the natural frequencies. It uses wavenumber functions which are defined as:

$$\begin{cases} k_a = (\frac{m\pi}{L})\left[\frac{h^2R^2}{12(1-\mu^2)}\right]^{1/4} \\ k_c = (\frac{n}{R})\left[\frac{h^2R^2}{12(1-\mu^2)}\right]^{1/4} \end{cases} ; \quad (23)$$

where k_a is the longitudinal (axial) wavenumber function and k_c is the circumferential wavenumber function.

By using these functions, a simplification of the previous equation for the natural frequencies can be obtained [28]. The equation becomes:

$$\omega_{mn} = \left[(k_a{}^2 + k_c{}^2)^2 + k_a^4 / (k_a{}^2 + k_c{}^2)^2\right]^{1/2} .2\pi f_r \quad (24)$$

where f_r is the ring frequency of the cylinder defined as: $f_r = (\frac{1}{2\pi R})\sqrt{\frac{E}{\rho_m}}$ where ρ_m is the density of the material, *E* is Young's modulus and *R* is the thickness of the structure. The normalized frequency ν_0 is defined as $\nu_0 = \frac{\omega_0}{2\pi f_r}$. The *k*-space diagram is a representation of *v*, k_a and k_c.

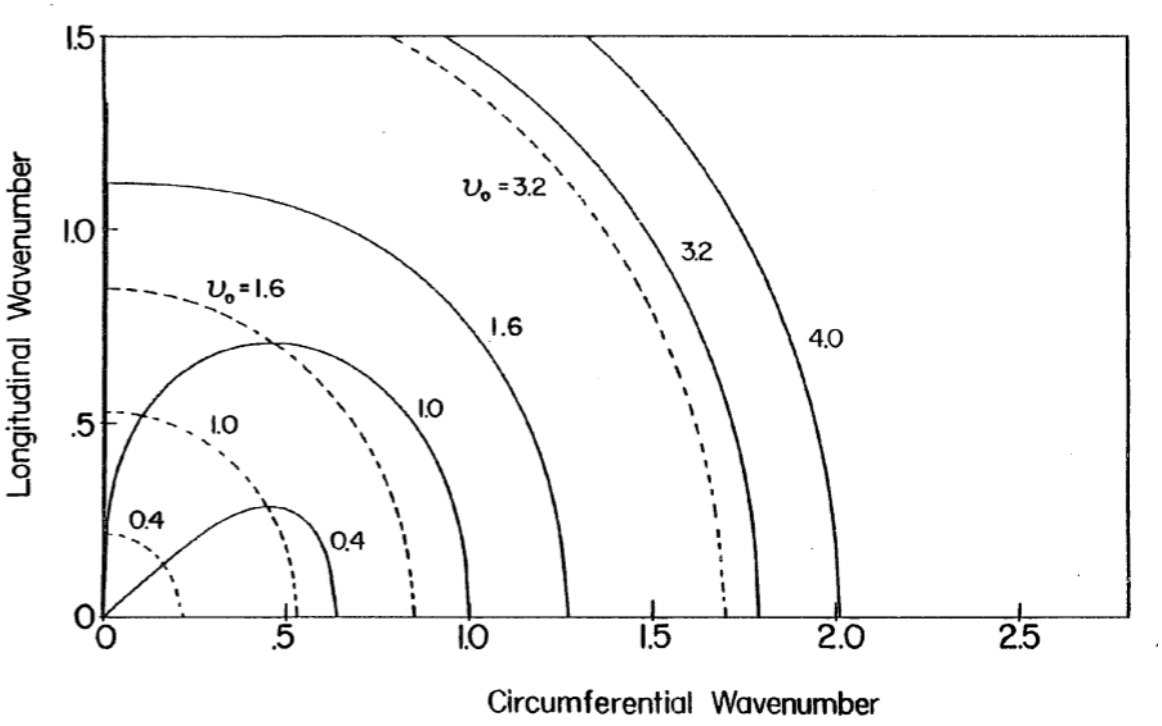

Figure 6: Wavenumber diagram [28].

Modal density:

Specific modes are represented by points in the wavenumber diagram distributed on a regular 2D lattice. Each mode occupies an area of the diagram equal to the product of the distance between mode points in each coordinate direction.

The modal density of a cylindrical shell is obtained from the number of modes and the bandwidth (units of mode/Hz). It has a peak value at the ring frequency. It can be defined as: $n(\omega) = \frac{dN}{d\omega}$ where N is the number of modes obtained by dividing the area occupied by the strip by the area of a unit mode.

2.3.2-Radiation from the cylinder:

The radiation efficiency [29] of a structure defines the efficiency of the sound radiation from this structure to the outside field. The formula determining radiation efficiency is:

$$\sigma = \frac{P_r}{\rho_0 c_0 S \langle v^2 \rangle}; \tag{25}$$

where P_r is the sound power radiated from the structure, $\rho_0 c_0$ is the characteristic impedance of the air, S is the surface area, and $\langle v^2 \rangle$ is the spatially averaged mean-square velocity of the radiating surface.

The frequency-averaged radiation efficiency depends on the number of modes resonant in a frequency band. These are called acoustically fast modes and acoustically slow modes: Acoustically fast modes are defined as the resonant modes where both k_a and k_c are less than k, while acoustically slow modes are ones where one or both the acoustical wavenumbers are greater than k. The radiation efficiency is higher for acoustically fast modes than acoustically slow ones.

Unlike a panel, a cylinder can have acoustically fast modes in all frequency ranges in which natural frequencies occur.

Acoustically fast modes are so far superior as radiators to any acoustically slow mode so that if they are present in a frequency band, the radiation from all acoustically slow modes in that band can be neglected. [25]

The radiation efficiency of the modes resonant in a frequency band of interest in a cylinder varies as follows:

For any frequency band that includes solely acoustically fast modes, the radiation efficiency of the cylinder is unity.

For any frequency band that includes both acoustically fast and acoustically slow modes, the radiation efficiency of the cylinder can be assumed to be given by the ratio of acoustically fast modes to the total number of modes resonant in the frequency band.

For any frequency band that includes solely acoustically slow modes, the radiation efficiency is given by the following equation [30]:

$$\sigma = \frac{(hR)^{1/2}\left[ln\frac{1+\left(\frac{f}{f_c}\right)^{\frac{1}{2}}}{1-\left(\frac{f}{f_c}\right)^{\frac{1}{2}}} + \frac{2\left(\frac{f}{f_c}\right)^{\frac{1}{2}}}{1-\left(\frac{f}{f_c}\right)}\right]}{\pi L[12(1-\mu^2)]^{1/4}(k_a^2+k_c^2)^{1/2}(1-\frac{f}{f_c})^{1/2}} \quad (26)$$

where f is the center frequency of the frequency band and f_c the critical coincidence frequency.

2.3.3-Cylinder response and Transmission Loss:

The transmission loss is defined as a measure of the sound insulation provided by a structural element. It can be written as: TL=10 log $[\frac{Incident\ acoustic\ power}{Transmitted\ acoustic\ power}]$.

In the case of a finite cylindrical shell, the transmission loss can be divided into two parts: resonant transmission and non-resonant transmission. Non-resonant transmission can be much more important at frequencies at which the resonant radiation is weak (therefore for acoustically slow modes). Resonant transmission is more important at high frequencies.

The resonant transmission can be derived from the power balance equations [29] and is given by the formula:

$$TL_{res} = -10\log_{10}[\frac{8\pi^2 c_0{}^2 n(\omega_0) R_{rad}{}^2}{\omega_0{}^2 m_s s^2 (2R_{rad} + R_{mech})}]; \qquad (27)$$

where $n(\omega_0)$ is the modal density in modes/Hz, R_{rad} the radiation resistance of all the modes resonant in the band, m_s the mass of the cylinder per unit area, *S* the radiating surface area and R_{mech} the mechanical resistance.

The non-resonant transmission loss formula depends on the frequency range being considered. Above the ring frequency, only the mass controlled modes are taken into account while below the ring frequency, both the mass and stiffness controlled modes are taken into account [24, 28].

The non-resonant transmission loss is given by two formulae depending on the frequency under consideration:

$$TL_{nr} = 8.33\log_{10}\left[[\nu_0{}^2(h/R)^2 E\rho_m / 4\rho_0{}^2 c_0{}^2][1-(\nu_0 f_r / f_c)^2]^2 + 2.3\right] \\ -3 + 20\log_{10}\left[\pi / 2\sin^{-1}\left[\nu_0[1-(\nu_0 f_r / f_c)^2]^{1/2}\right]^{1/2}\right]; \quad (28)$$

for ν_0 <1, below the ring frequency,

and

$$TL_{nr} = 8.33\log_{10}\left[[\nu_0{}^2(h/R)^2 E\rho_m / 4\rho_0{}^2 c_0{}^2][1-(\nu_0 f_r / f_c)^2]^2 + 2.3\right] - 3; \quad (29)$$

for ν_0 >1 above the ring frequency.

The total transmission loss (TL) of the cylinder is calculated from the energy sum of the resonant transmission loss and the non-resonant transmission loss.

2.3.4- Computational implementation:

The parameters explained in this theoretical part were used in a Matlab program to calculate transmission loss theoretically. This program is given in the Appendix.

The implementation is different from the one used for the panel since it uses the wavenumber diagram. One first enters the specific parameters of the cylinder that are being studied, and then one starts with the bandwidth analysis which sets the frequency band considered.

The program is used to solve the equation:

$$k_a^8 + (4k_c{}^2)k_a^2 + (6k_c^4 + \nu_0{}^2 + 1)k_a^4 + (4k_c^6 - 2\nu_0 k_c^2)k_a^2 + (k_a^8 - \nu_0{}^2 k_a^4) = 0\,; \qquad (30)$$

which is expanded from the equation: $\omega_{mn} = \left[(k_a{}^2 + k_c{}^2)^2 + k_a^4 / (k_a{}^2 + k_c{}^2)^2\right]^{1/2} .2\pi f_r$. Then, for each given frequency ν_0, 300 values for k_a and for k_c are taken. The acoustically fast, acoustically slow, and acoustically fast and slow modes were also isolated to be able to use the correct formulae for transmission loss previously given and finally to obtain a theoretical value to compare with the experiments.

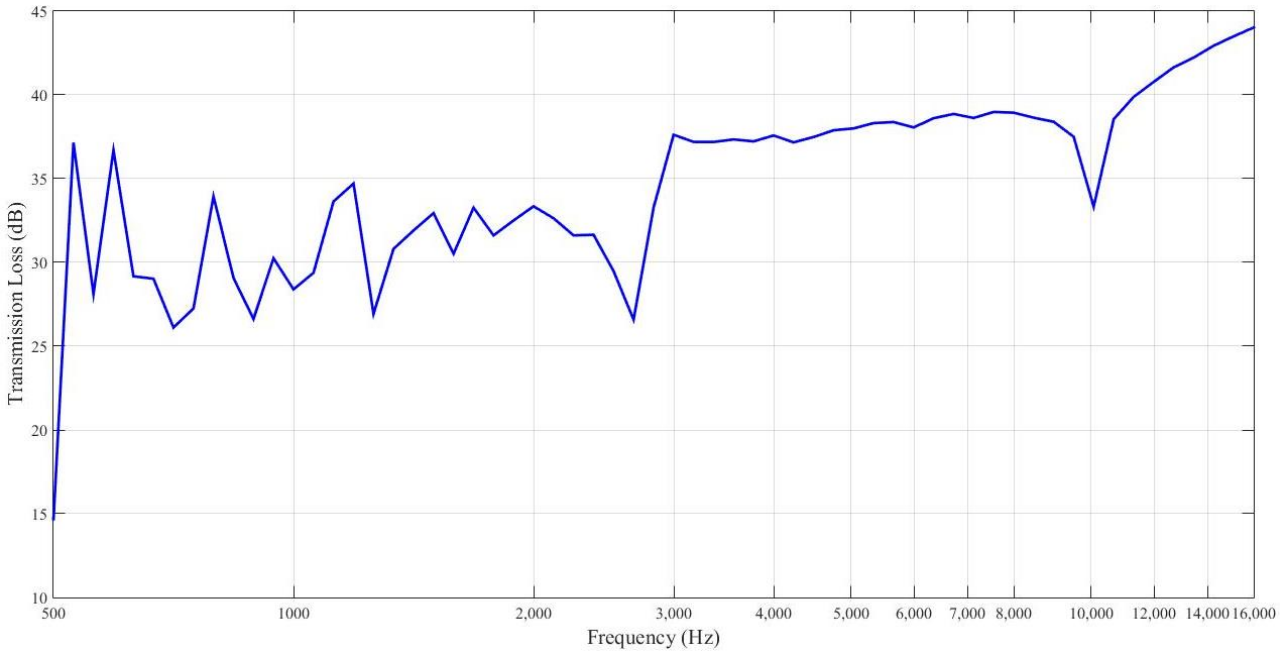

Figure 7: Cylinder theoretical transmission loss.

The thin cylindrical shell used for the program has an outside diameter of 0.6096 m with a wall thickness of 1.27 mm. The cylindrical shell was made of galvanized steel metal with an

estimated density of 7,850 kg/m^3, a Young's modulus of 200 GPa, and a Poisson's ratio of 0.28. The overall length of the cylindrical shell is 2.0574 m with a 19.05 mm wide plywood disk placed inside both ends. The inside distance between the two plywood disks was 2.0066 m.

The program was run for frequencies ranging from 500 Hz to 16,000Hz where SEA is more reliable. Two dips can clearly be seen at the ring frequency (2,636 Hz) and at the critical frequency (10,118 Hz) of the cylinder. The sound transmission loss at these frequencies is lower than it is at the other frequencies and does not follow "mass law" theory.

The program was also used to obtain the cylinder response relative to mass law as shown in Figure 8:

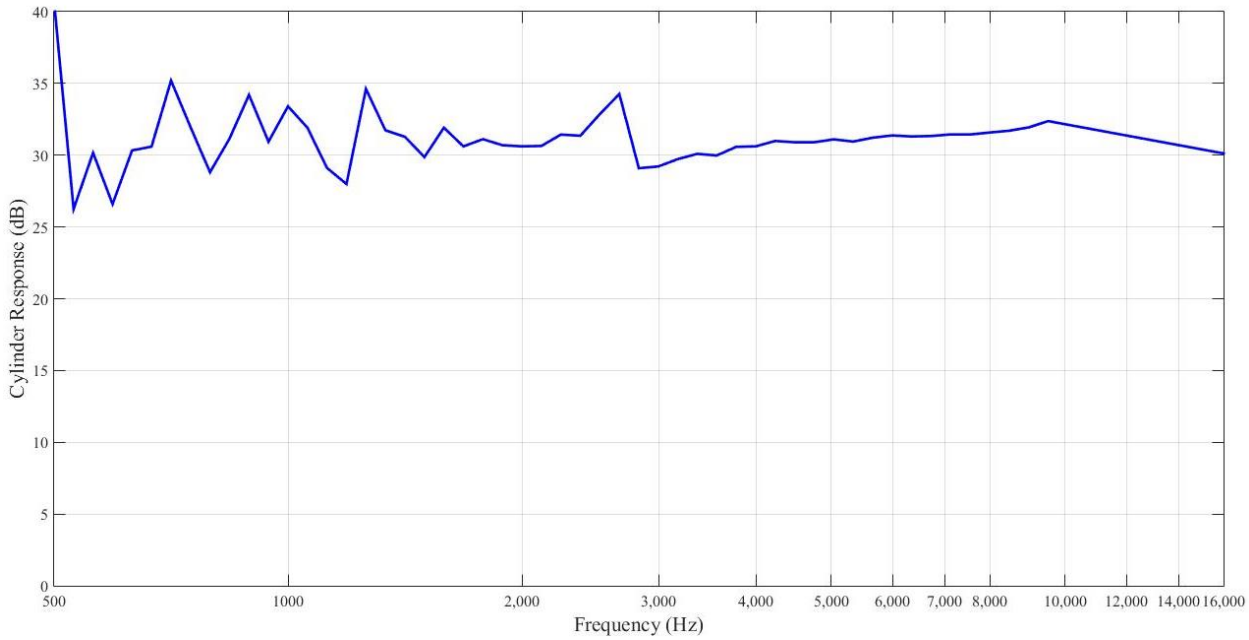

Figure 8: Cylinder response relative to mass law.

Chapter 3: Experimental investigations of the transmission loss

3.1- Reverberation time measurements:

Measuring the reverberation time T_R of the receiving room was of prime importance in the experimental part of this study, since it was later used to calculate the transmission loss for each structure. The reverberation time of a structure is defined as the time necessary for the sound to decrease to a level of 60 decibels below its original steady level when a sound source ceases. Pulse LabShop software and hardware, produced by Bruel & Kjaer [31], a company specialized in acoustical instrumentation was used to collect and process the data for this and all of the other sets of experiments. The software provides a program to measure the reverberation time using sound decay measurements. Many tests were conducted in which parameters were modified to estimate the reverberation time of the room:

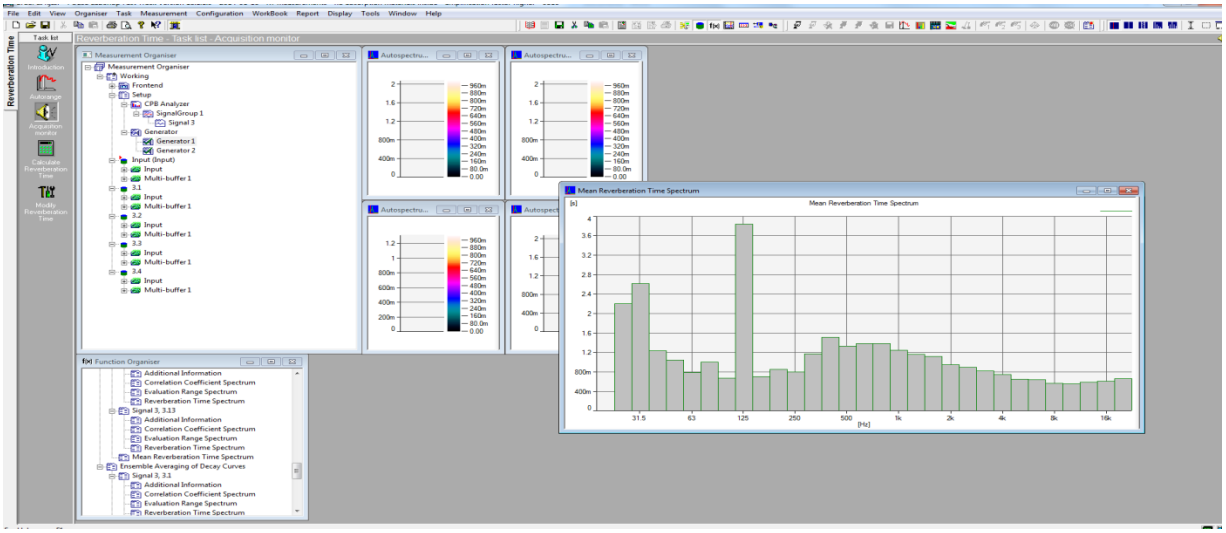

Figure 9: Program to measure the reverberation time of the receiving room.

The experiments were conducted with absorption material in the room and then without it. Then the amplification factor of the loudspeakers was changed. The reverberation time values obtained were relatively similar despite the fact that these parameters were being modified. It was concluded that the experiments gave a correct estimate of the reverberation time that could later be used to calculate the transmission loss of the panel and of the cylinder.

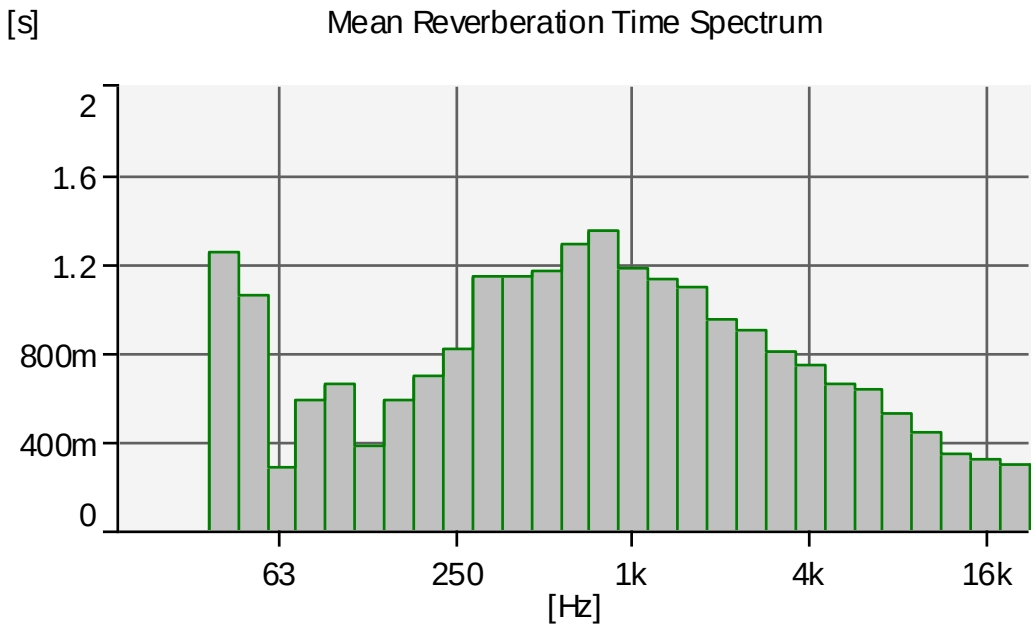

Figure 10: Reverberation Time of the reception room in 1/3 octave band.

3.2-Panel experiments:

3.2.1-Experimental setup:

The thin flat panel under study was 1.04 m long, 0.609 m wide and 0.00127 m thick. The panel was made of galvanized steel metal with an estimated density of 7,850 kg/m^3, a Young's modulus of 200 GPa, and a Poisson's ratio of 0.28.

Figure 11: Panel used for the experiments.

The same experimental setup was used for both sets of experiments. The flat panel was clamped between two reverberation rooms of the same dimensions. Large loudspeakers and a pressure source were placed in one of the rooms, which was considered to be the source room for the noise. It was otherwise empty. The calculated critical frequency was 10,118 Hz, both these noise sources were needed to provide enough sound power so that the sound pressure level

produced would be sufficiently above the background noise. The second room, or receiving room was also empty.

Figure 12: Loud speakers and turbulent flow pressure tubes.

3.2.2- Transmission suite experiments on the panel:

The two room method is widely used to evaluate the transmission loss (TL) of a structure and consists of having the structure placed between a source room and a receiving room as described above. A microphone was placed in the source room to measure its sound pressure level, called the incident sound pressure level. Another microphone was placed in the receiving room to measure the received sound pressure level. The measurements were taken in different locations in both rooms to obtain a space-average of the sound pressure level in each room. Sound fields in the two rooms were reverberant, allowing the calculation of the noise reduction of the panel [31].

First however, the background sound pressure needed to be measured to confirm that the sound pressure levels in each room were sufficiently above the background noise so that the results could be considered acceptable. To measure the background sound pressure, the microphones were placed in different locations of each rooms with no noise sources present. The following results were obtained:

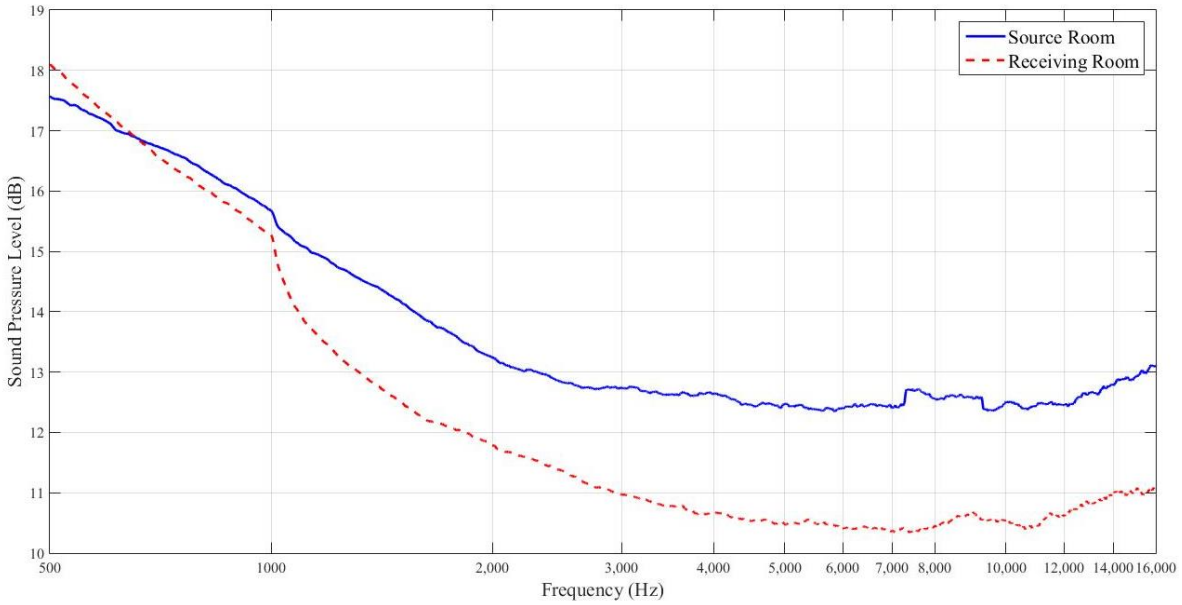

Figure 13: Background sound pressure levels in the source room and the receiving room.

As Figure 13 shows, the background sound pressure level measured did not exceed 16 dB in the frequency range of interest.

Then, using both the loudspeakers and the turbulent flow pressure tubes as noise sources, and placing the microphone at five different locations for each room, the sound pressure level in both rooms was measured then the space-average of each of the measurements was calculated.

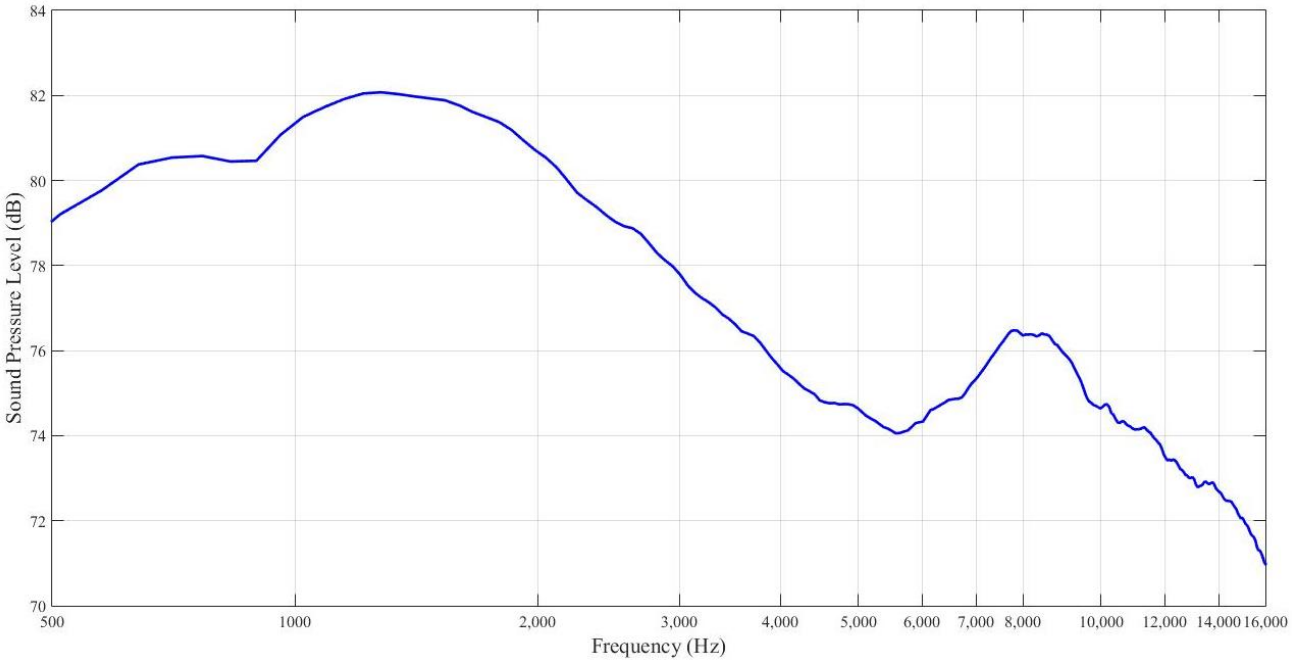

Figure 14: Sound pressure level in source room

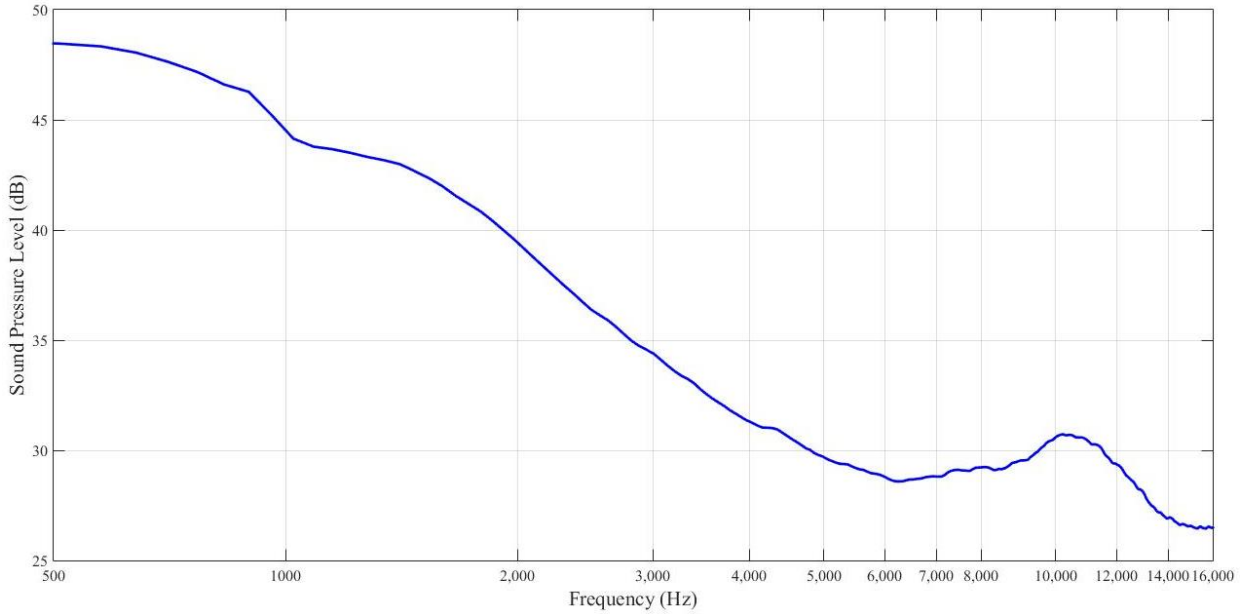

Figure 15: Sound pressure level in receiving room.

The sound pressure level in the source room was between 70 dB and 82 dB in the frequency range of interest and between 25 dB and 45 dB in this frequency range for the receiving room. The sound pressure level drop was very noticeable (at least 25 dB) with a peak at the frequency 10,200Hz which is very close to the panel's calculated critical frequency.

By comparing the sound pressure levels when the noise sources were turned and the background sound pressure level, it was concluded that the measurements were not contaminated by background noise:

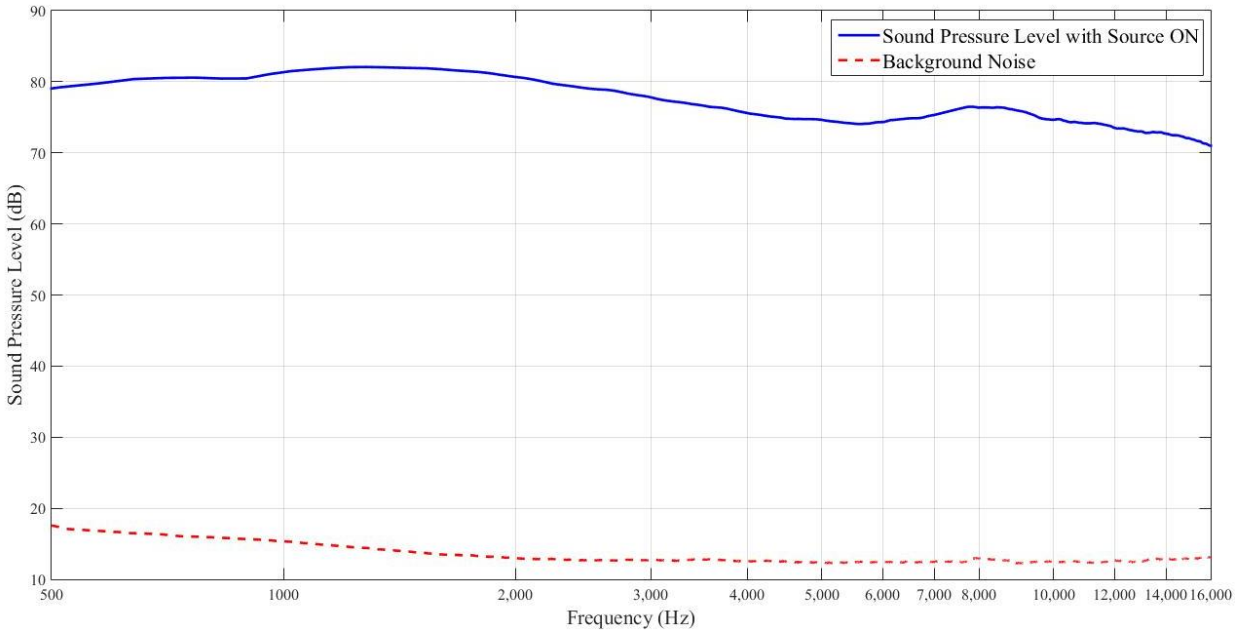

Figure 16: Sound pressure level and background noise in the source room.

In the source room, as Figure 16 shows, the background sound pressure level was at least 40 dB lower than the sound pressure level with the noise source on.

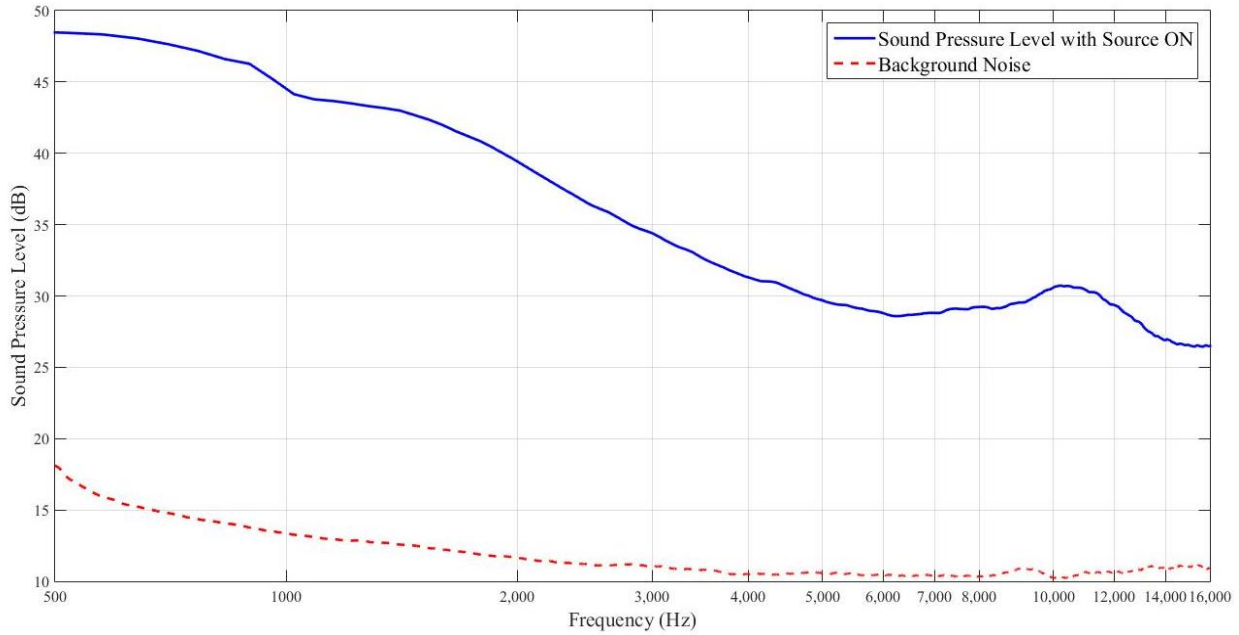

Figure 17: Sound pressure level and background noise in receiving room.

In the receiving room, as Figure 17 shows, the background sound pressure level was at least 10 dB lower up to 5,000 Hz than the sound pressure level with the noise sources were turned on in the source room.

The noise reduction (NR) was calculated by subtracting the obtained sound pressure level from one another, using the formula: $NR = 10\log_{10}(\frac{P_{in}}{P_{out}})$ Where P_{in} is the sound pressure in the source room and P_{out} is the sound pressure in the receiving room. The noise reduction was then plotted for the desired frequency range.

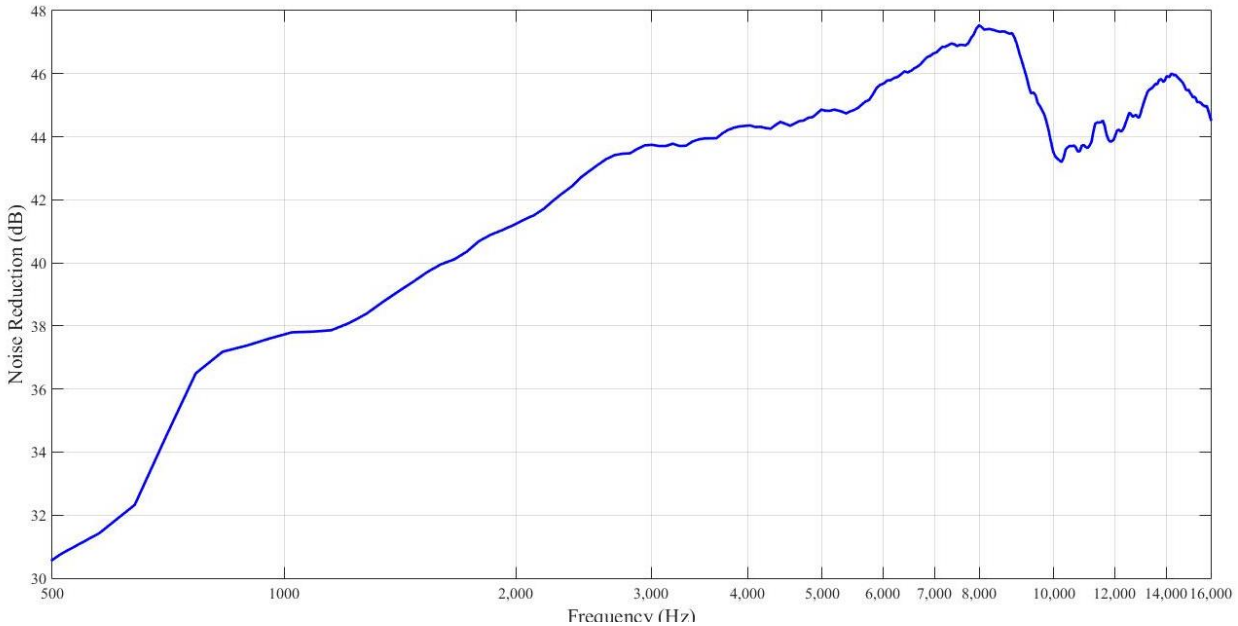

Figure 18: Panel noise reduction.

As Figure 18 shows, the noise reduction of the panel increases with a slope of about 6 dB per doubling of frequency up to the critical frequency where a dip can be observed.

The second parameter needed to calculate the transmission loss using the noise reduction is the reverberation time T_R. This was measured previously. So the transmission loss was calculated using the following formula: $TL = NR + 10\log_{10}(\frac{Sc_0T_R}{24V\ln(10)})$; where V is the volume of the reception room, S the surface area of the panel and c_0 the speed of sound in the air. The following is the result obtained:

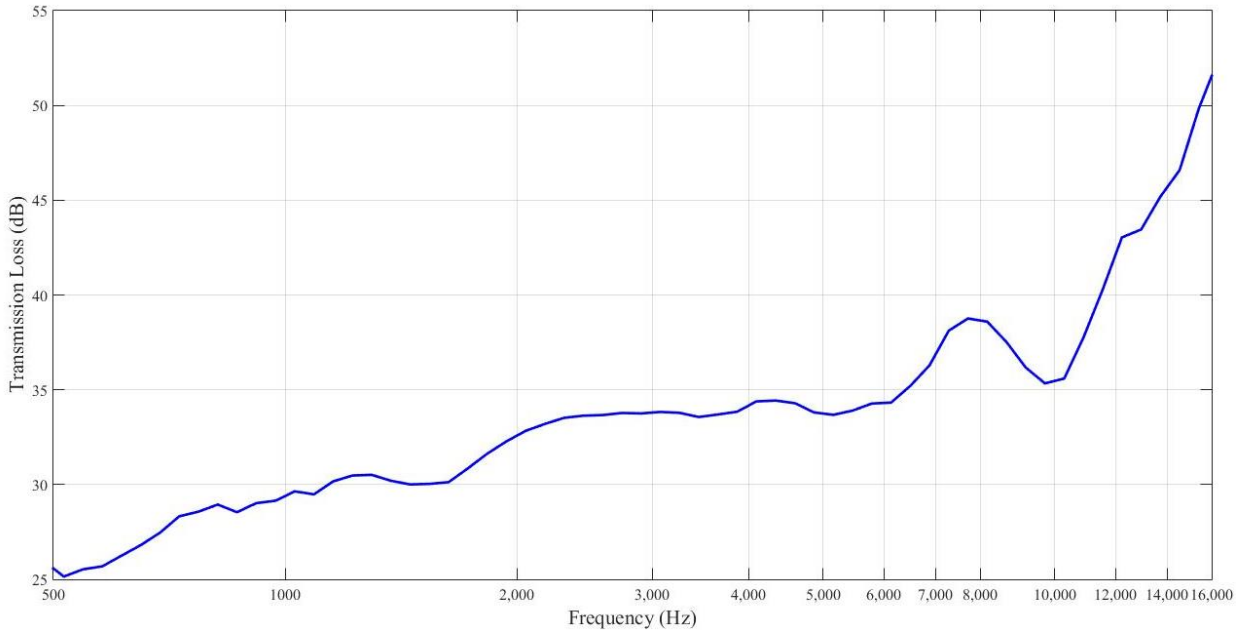

Figure 19: Panel transmission loss using sound pressure level measurements.

Figure 19 shows a dip near the critical frequency (about 10,100 Hz) where the transmission loss decreases then increases. The results at low frequencies do not seem to be as good as expected. A correction was made to take into account the effect of the background noise when calculating the transmission loss for the panel.

The sound pressure level measurements were also used to plot the experimental response of the panel relative to mass law. The acceleration of the panel was measured using an accelerometer placed in five different locations, these results were then averaged to obtain the surface average acceleration level on the panel. These results were used to plot the response of the panel relative to mass law:

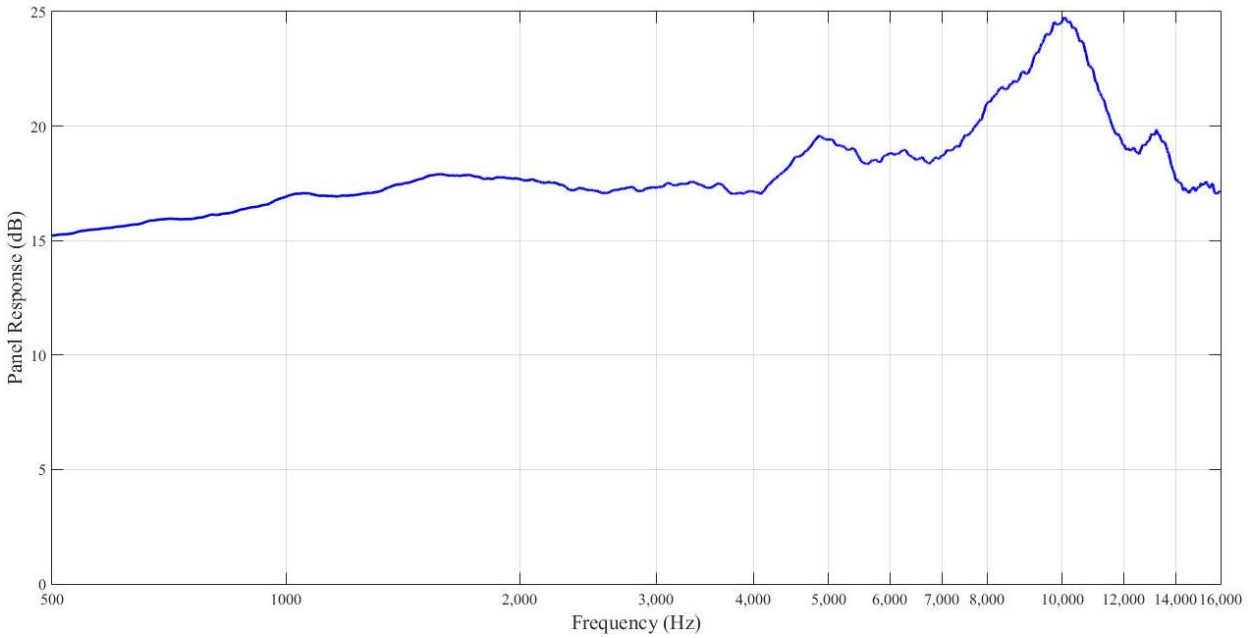

Figure 20: Experimental panel response relative to mass law.

3.2.3-Sound intensity experiments on panel:

Using the same experimental setup, a second method was applied to calculate the transmission loss of the panel. This method uses a sound intensity probe to measure the transmitted intensity in the receiving room when the panel is subjected to a noise source in the source room. The sound intensity in the source room is calculated using the sound pressure level in the source room.

For the experiment, the sound pressure level was measured in the source room at five different locations of the room, space-averaged, then converted into incident intensity on the panel using the formula:$I_{in} = \frac{P_{in}^2}{4\rho_0 c_0}$. This is valid under the assumption that the sound field in the source room is reverberant and diffuse. The following figure, Figure 21, shows the results obtained:

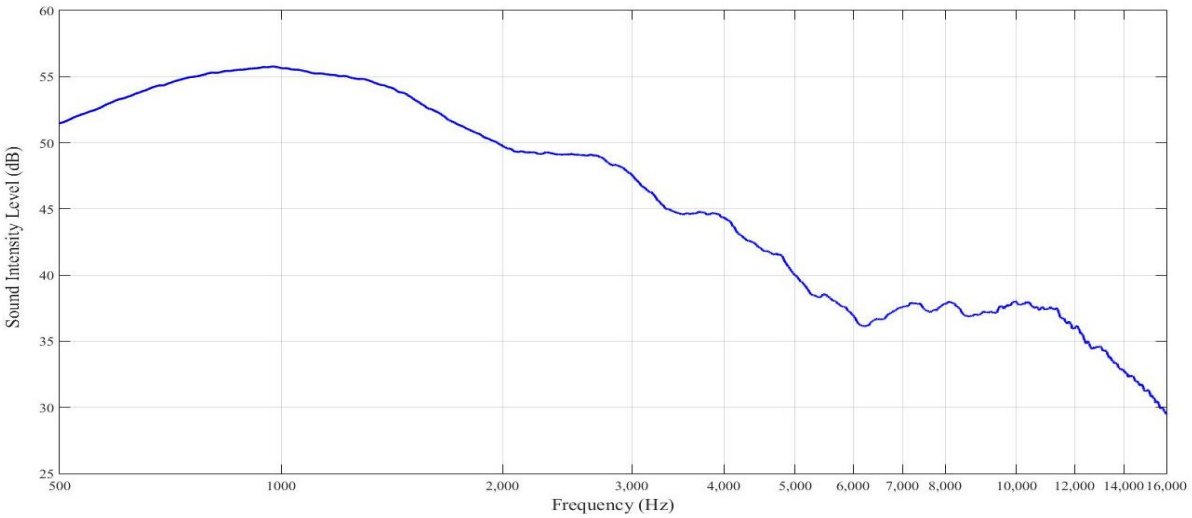

Figure 21: Calculated Intensity incident on panel in source room.

The sound intensity probe was used to measure the sound intensity transmitted through the panel in the receiving room. The probe was placed close enough to the panel so that the direct field was dominant. The experiment was repeated five times and the results were averaged. The procedure for sound intensity measurements using the sound intensity probe is further described in the Appendix. The following results were obtained for the transmitted sound intensity:

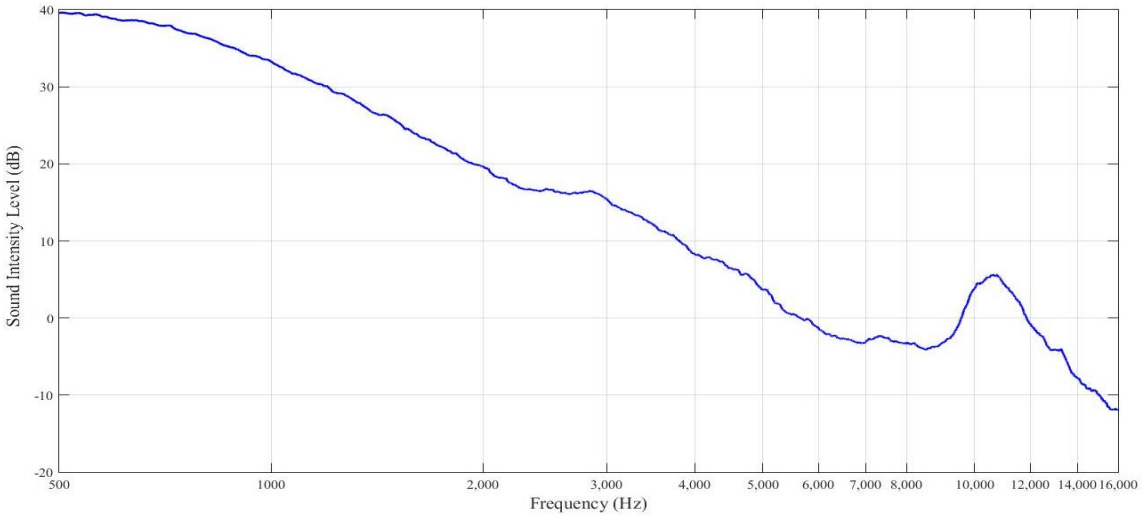

Figure 22: Sound intensity transmitted through the panel.

With this second method, a peak in the transmitted intensity can also be seen at the calculated value of the critical frequency. It is also noticeable that the sound intensity level in the receiving room transmitted through the panel is much lower than the sound intensity level incident on the panel in the source room.

To make sure the sound intensity results were reliable, the background sound intensity in the source room was calculated using the background sound pressure level previously measured and compared to the incident sound intensity level. The background sound intensity in the receiving room was also measured and compared to the transmitted sound intensity. The results are shown in Figures 23 and 24.

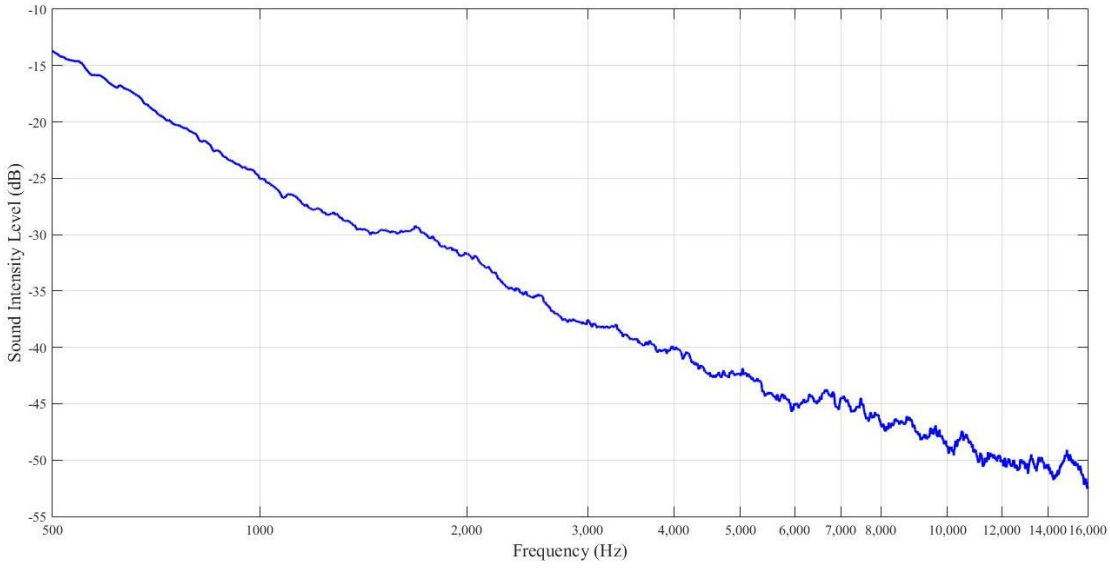

Figure 23: Background sound intensity level in the source room.

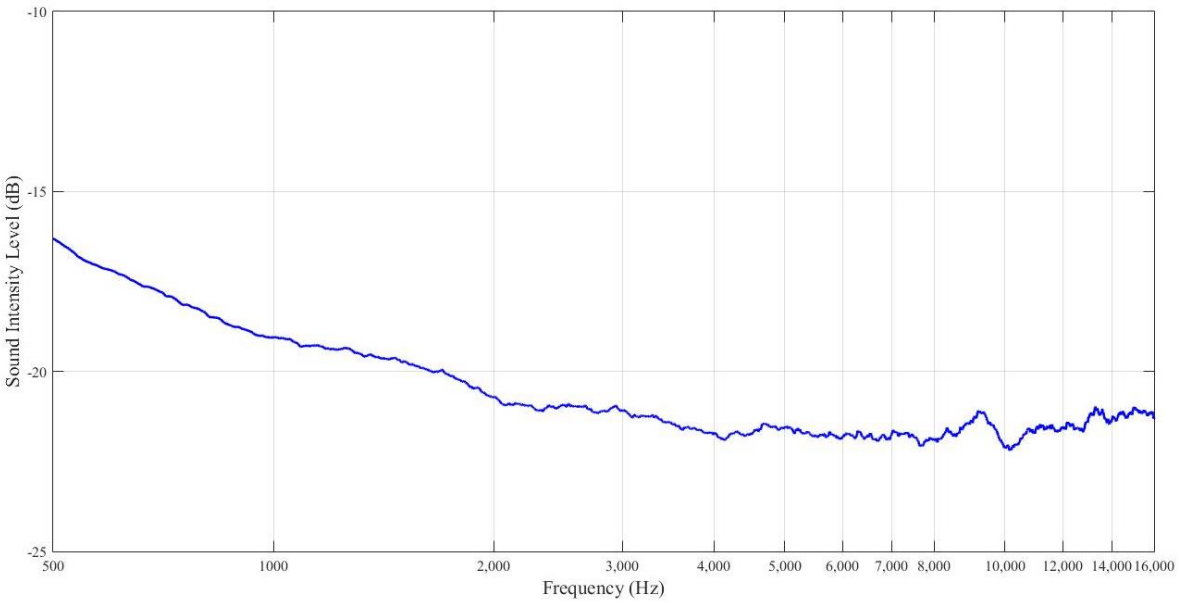

Figure 24: Background sound intensity level in the receiving room.

As Figures 23 and 24 show, the background sound intensity levels in both the source room and the receiving room are low. These measurements were compared to the sound intensity level measurements with the loudspeakers turned on to make sure the intensity measurements are not contaminated by background noise or instrument noise for the frequency range of interest:

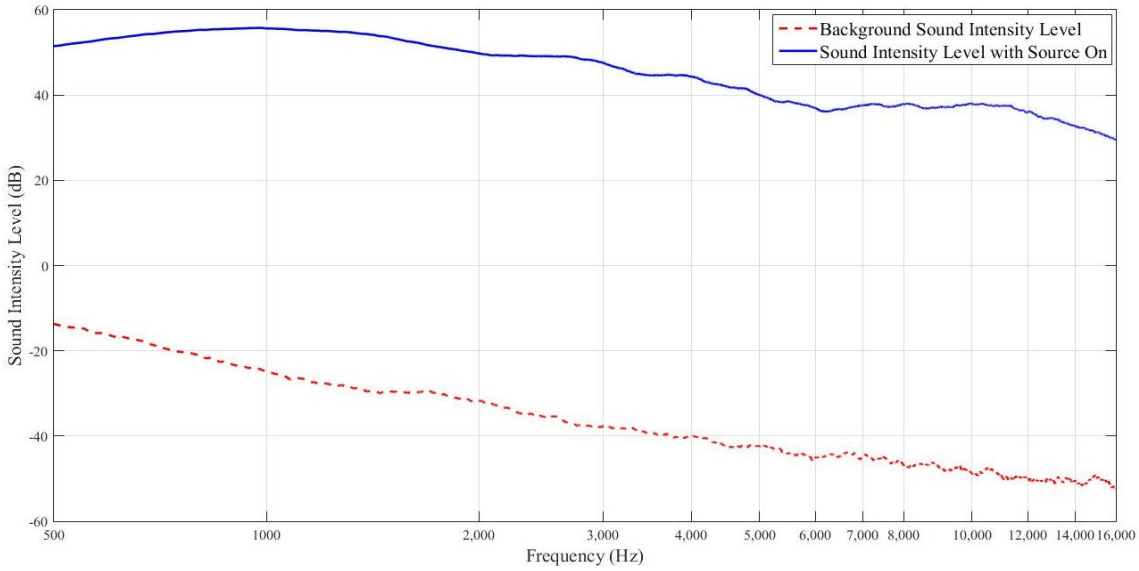

Figure 25: Background sound intensity level and sound intensity level with the loudspeakers on in the source room.

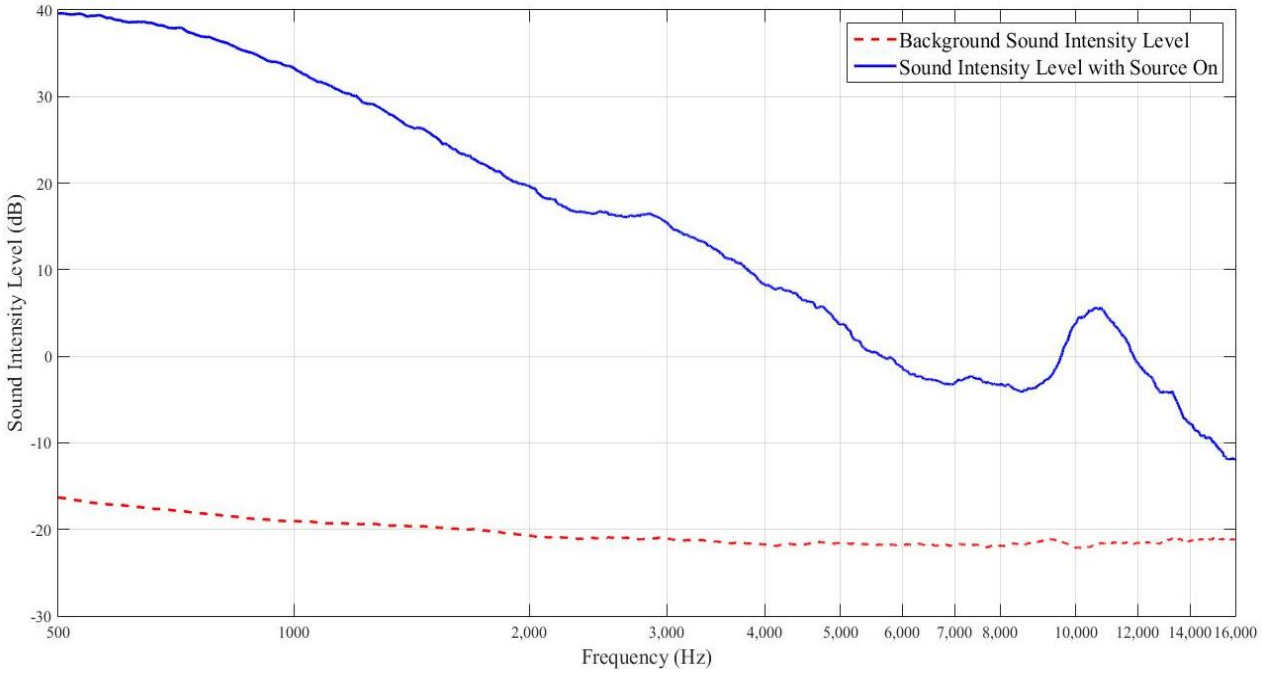

Figure 26: Background sound intensity level and sound intensity level with the loud speakers on in the receiving room.

Then, using the definition for transmission loss: $TL = 10\log_{10}(\frac{I_{in}}{I_{out}})$, where $I_{in}$is the incident sound intensity and I_{out} is the intensity transmitted through the panel into the receiving room, the transmission loss was calculated and the following results in Figure 27 were obtained:

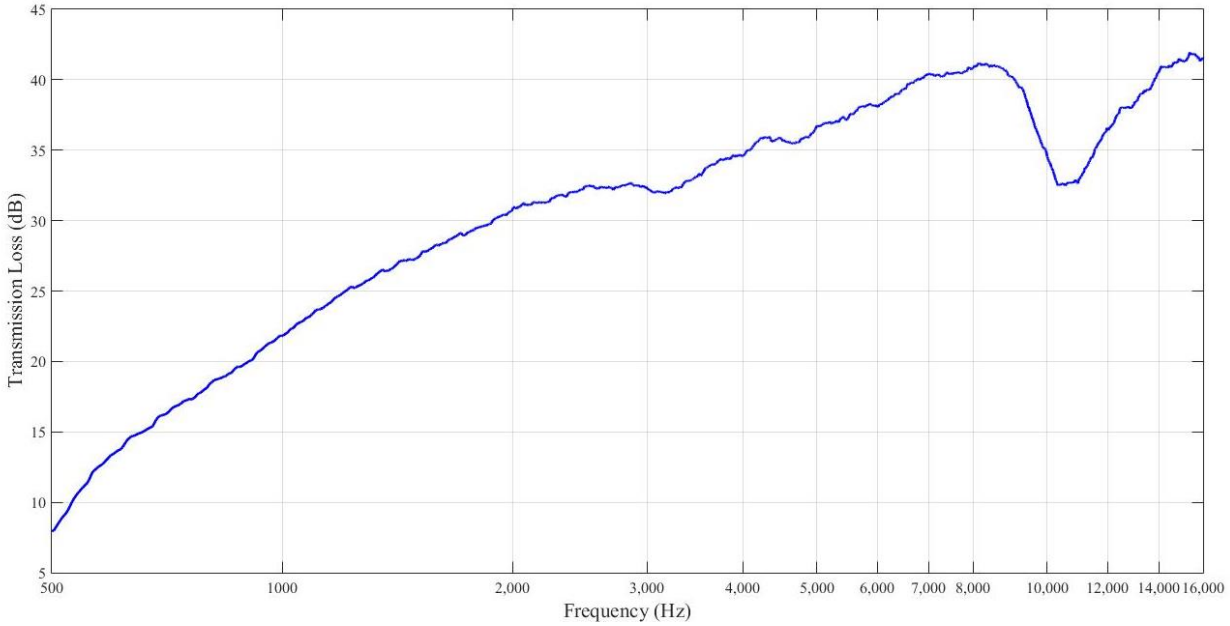

Figure 27: Panel transmission loss using sound intensity.

Below the critical frequency, the transmission loss gradually increases with a slope of 6 dB per doubling of frequency. Then at the critical frequency, the measurements of TL show a pronounced dip at the critical frequency where the transmission loss decreases then gradually increases again with an increase in slope.

3.3-Cylinder experiments:

3.3.1-Experimental setup:

The thin cylindrical shell under study has an outside diameter of 0.6096 m with a wall thickness of 1.27 mm. The cylindrical shell is made of galvanized steel metal with an estimated 7,850 kg/m^3 density, 200 GPa Young's modulus, and 0.28 Poisson's ratio. The overall length of

the cylindrical shell is 2.0574 m with a 19.05 mm wide plywood disk placed inside both ends. The interior distance between the two plywood disks is 2.0066 m.

Figure 28: Cylindrical shell used during the experimental investigation.

The same experimental setup was used for both sets of experiments, the cylinder was suspended in a reverberant room with two loudspeakers + tweeters and a microphone inside the cylinder that could be rotated.

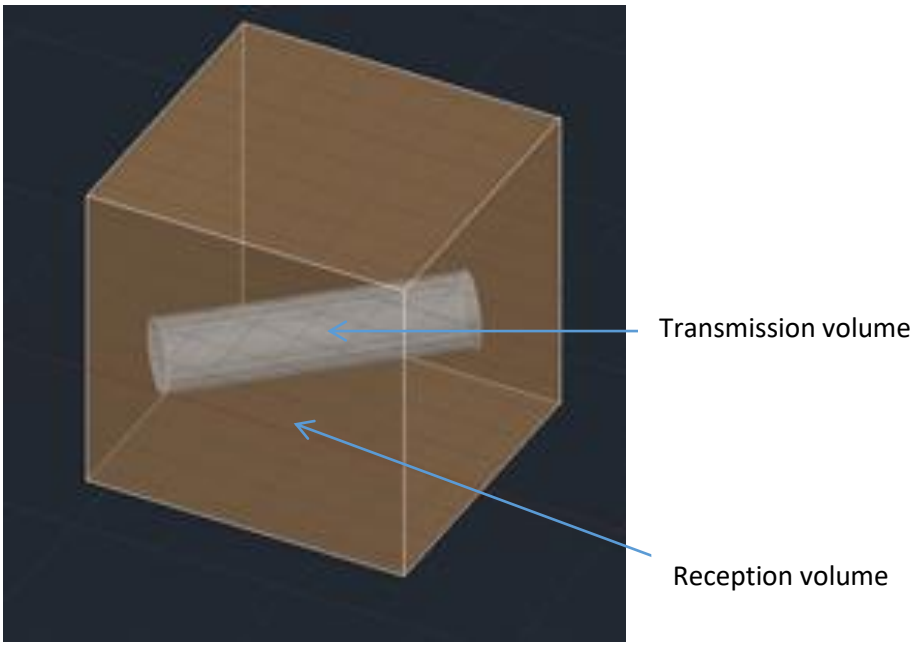

Figure 29: Model of the transmission and reception volumes.

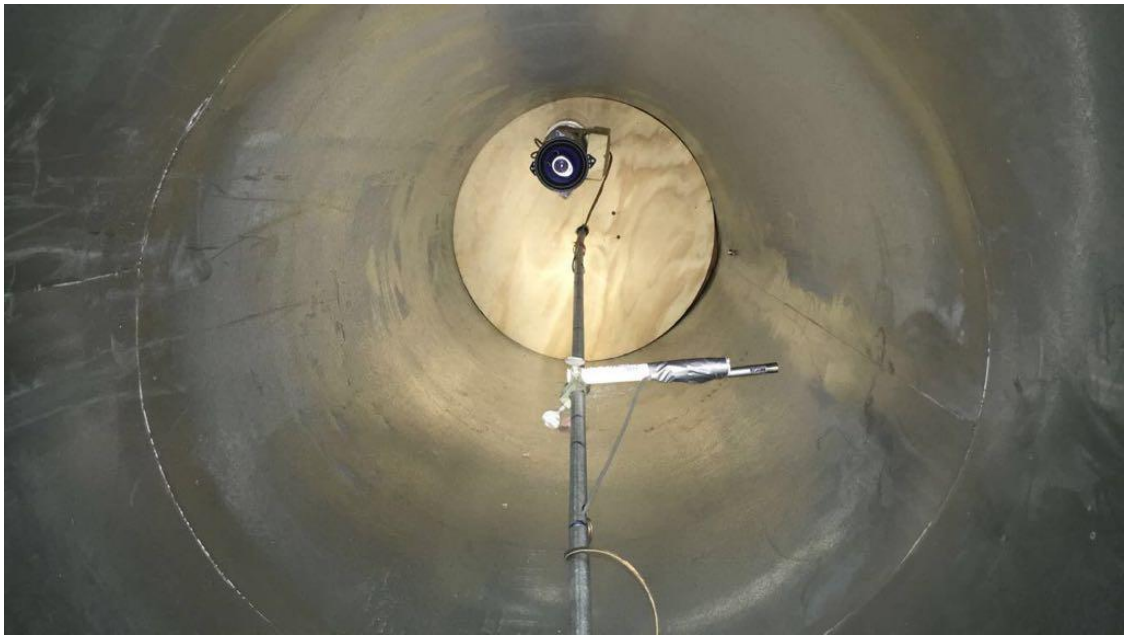

Figure 30: Loudspeaker and tweeter inside the cylinder.

3.3.2-Transmission suite experiments on the cylinder:

The first method used, also referred to as the two room method, which consists of using two reverberation spaces separated by the structure studied (in our case the cylindrical shell) which was previously described. In this method, the source room and the receiving room are also called the transmission room and the reception room. When using loudspeakers inside the cylindrical shell, the reception room is the room in which the cylinder is located and the transmission room is the inside of the cylinder. First, the background sound pressure level was measured inside and outside the cylinder to confirm the sound produced and transmitted is high enough above the background noise, so that the results can be considered acceptable.

To measure the background sound pressure level, the loudspeakers inside the cylinder were turned off and the microphones were placed at five different locations in the room and the cylinder. The following results were obtained:

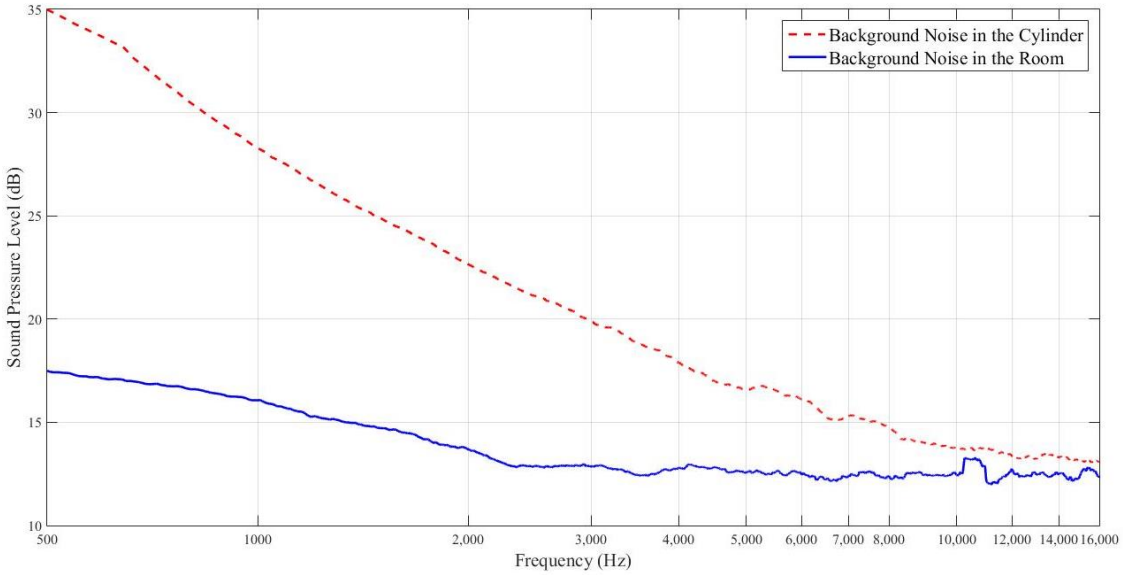

Figure 31: Background sound pressure levels for the room and for the cylinder.

The background sound pressure level measured did not exceed 30 dB in both the transmission room and the reception room.

Then, using the source, sound pressure levels were measured inside the cylinder and in the receiving room for five different locations and space-averaged:

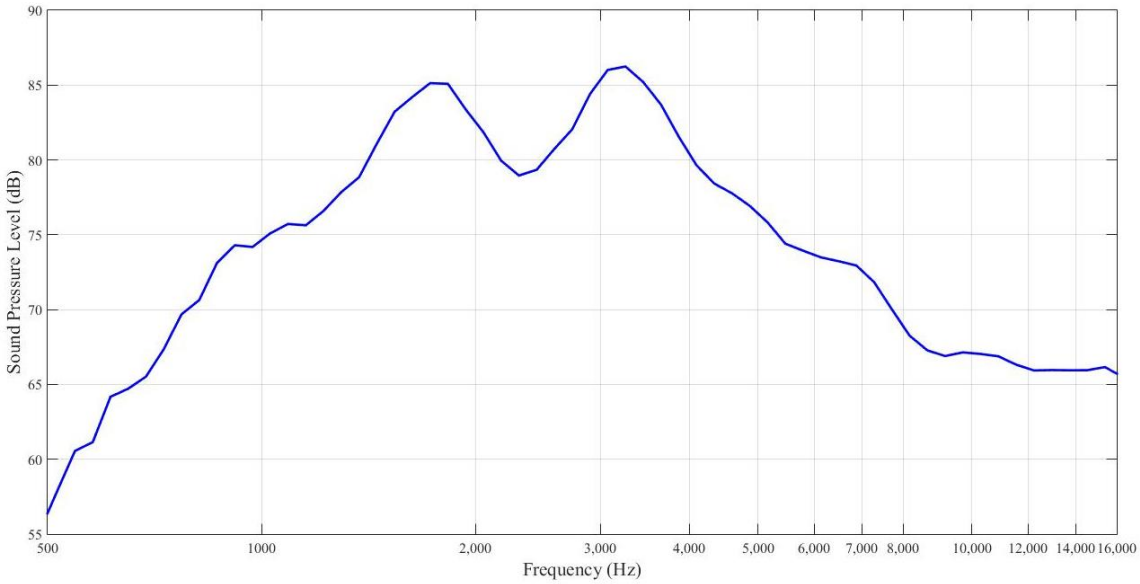

Figure 32: Sound pressure level inside the cylinder.

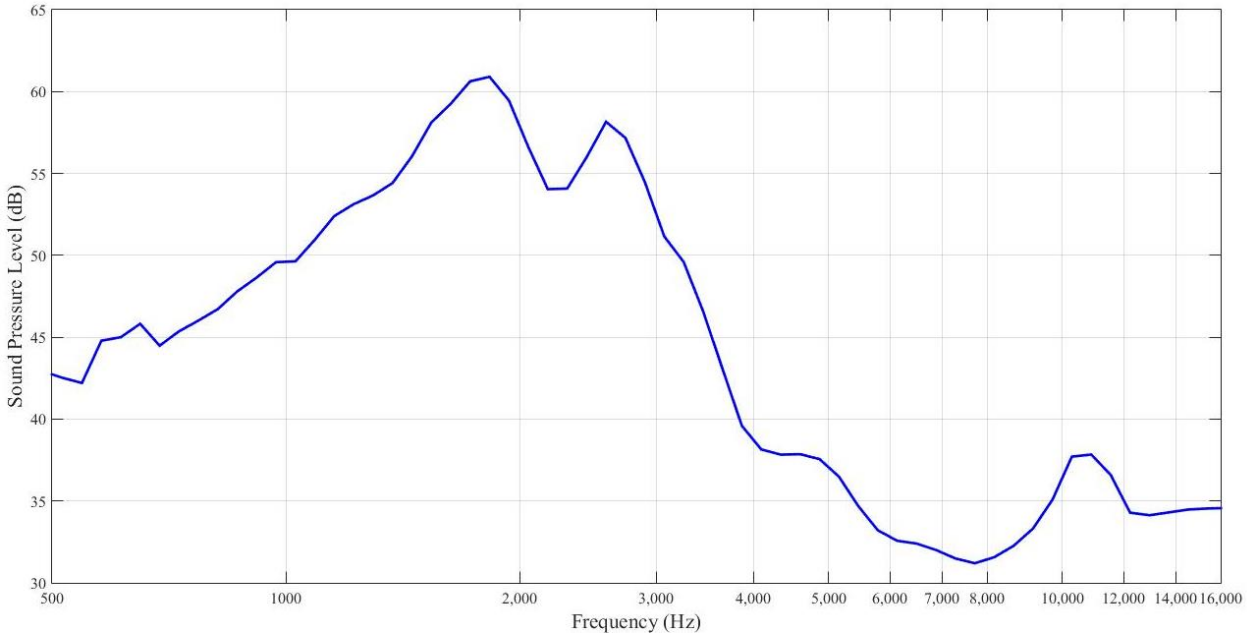

Figure 33: Sound pressure level in the receiving room.

The sound pressure level inside the cylinder was between 65 dB and 85 dB in the frequency range pf interest for the source room and between 30 dB and 65 dB in the same frequency range for the receiving room. The sound pressure level drop was very noticeable (at least 25dB) with a clear peak at a frequency of about 10,100 Hz which is very close to the calculated critical frequency. By comparing the sound pressure levels when the source is used and the background sound pressure levels, it is clear that the measurements are reliable:

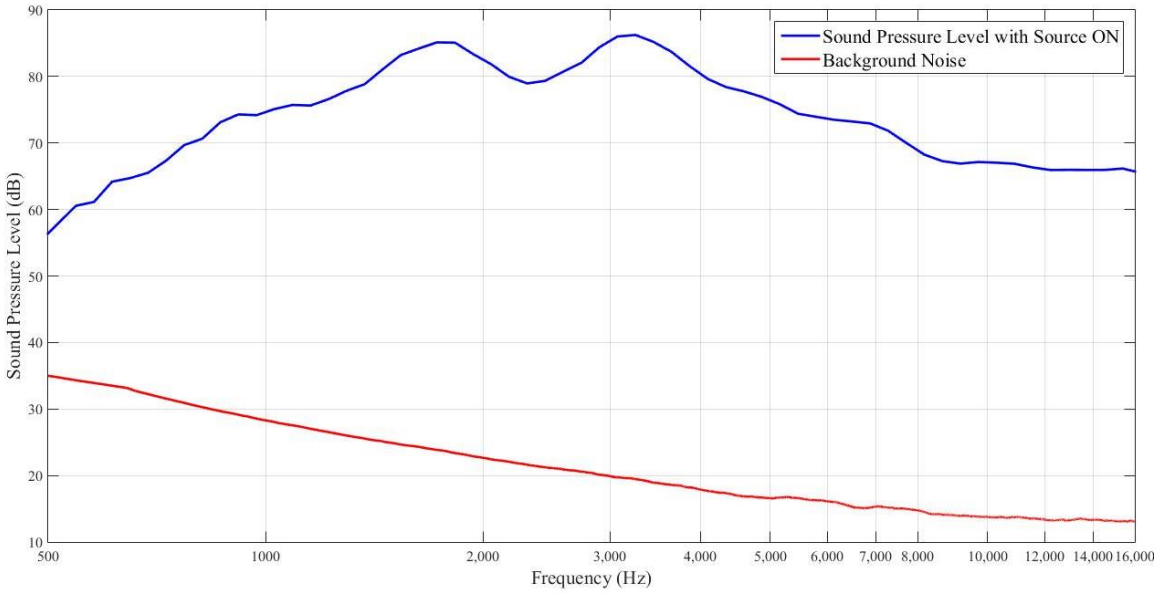

Figure 34: Sound pressure level and background noise inside the cylinder.

Inside the cylinder, the background sound pressure level was at least 60 dB below the sound pressure level with the source at all frequencies. This result is similar to the one obtained for the panel.

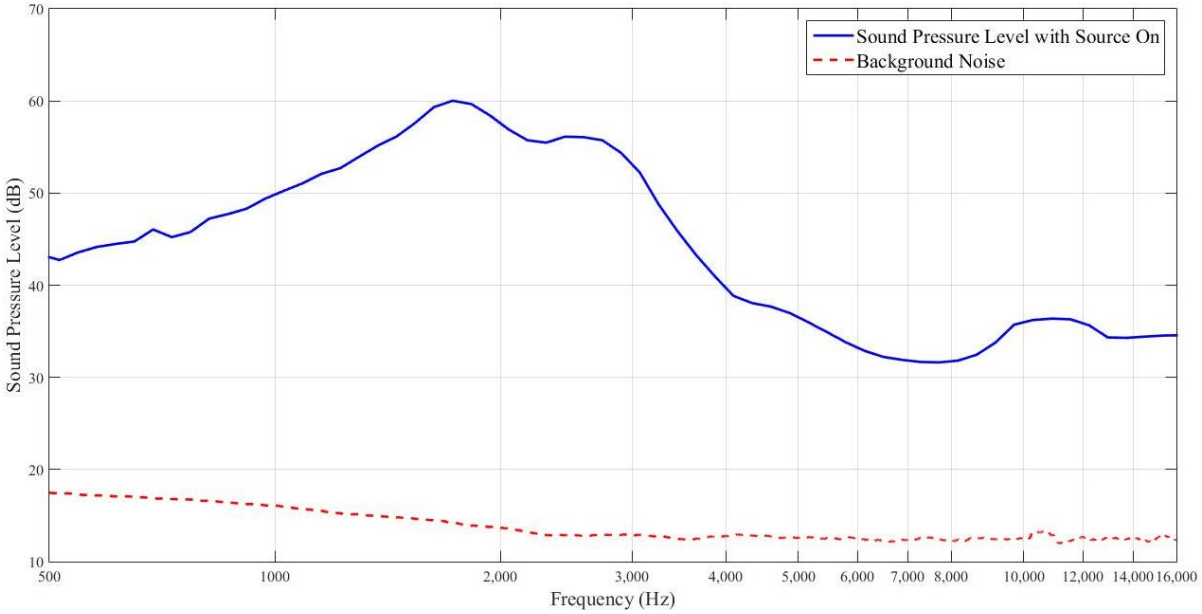

Figure 35: Sound pressure level and background noise in receiving room.

In the receiving room, the background sound pressure level was at least 25 dB below the sound pressure level with the source turned on at all frequencies. This difference was higher than the one obtained for the panel.

Then, the measured sound pressure level in the transmission room was subtracted from the measured sound pressure level in the reception room to obtain the noise reduction (NR). The experimental method used was similar to the one used for the panel. The results obtained were plotted in the following Figure 36:

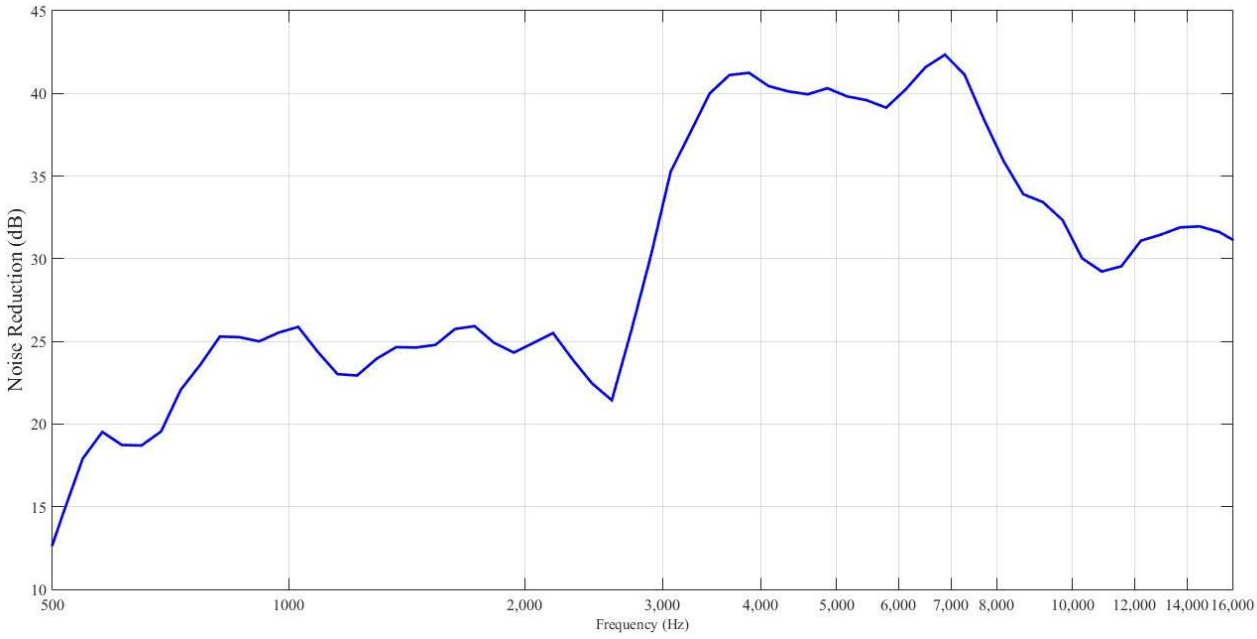

Figure 36: Cylinder noise reduction.

Two dips can clearly be observed for the cylinder noise reduction: one at the experimental ring frequency of the cylinder and another one at the experimental critical frequency. These two frequencies coincide with the calculated ring and critical frequencies.

The reverberation time, previously measured is also needed to calculate the transmission loss and is then given by the formula:

$$TL = NR + 10\log_{10}(\frac{Sc_0T_R}{24V\ln(10)});$$

where V is the volume of the reception room, S the surface area of the cylinder and c_0 the speed of sound in the air.

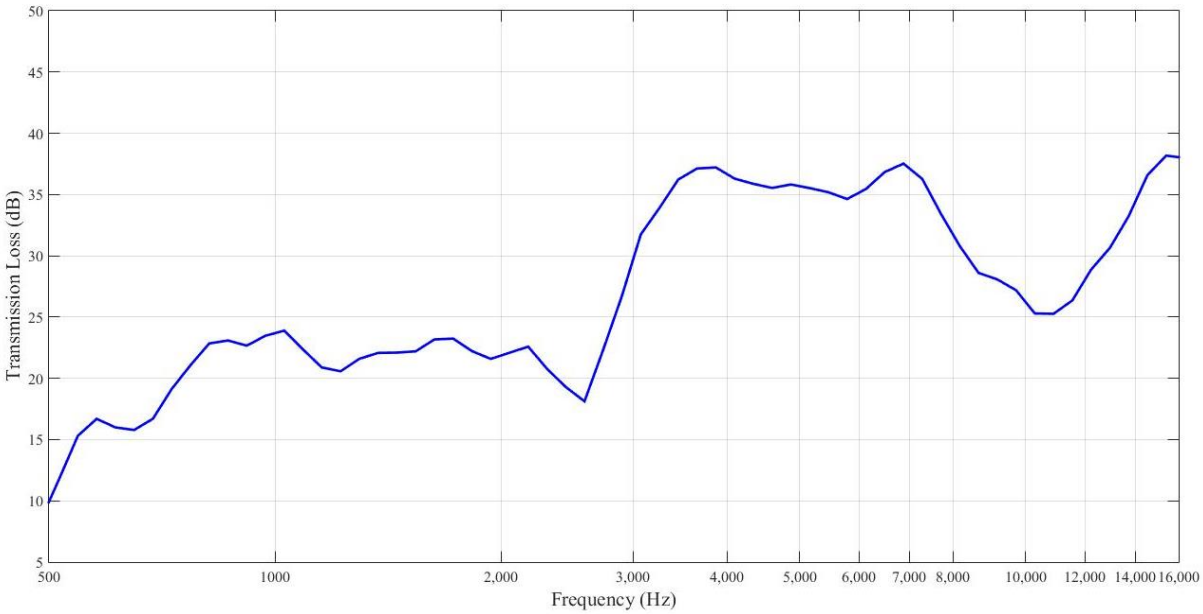

Figure 37: Cylinder transmission loss using the sound pressure levels.

The figure shows that the transmission loss is very low below the ring frequency, then a dip can be observed at the ring frequency. The transmission loss increases up to the critical frequency where the second dip can be observed, then the transmission loss becomes higher.

3.3.3-Sound intensity experiments on the cylinder:

The second method used to calculate the transmission loss is the intensity method. It consists of measuring the sound pressure level inside the cylinder using the microphone placed inside and the intensity measured outside the cylinder using a sound intensity probe [32, 33]. Then the sound pressure level results calculated were used to estimate the intensity inside the cylinder. Using the previously given formula the transmission loss TL was calculated:

$$TL = 10\log_{10}(\frac{I_{in}}{I_{out}}).$$

The advantage of this second method is that only one sound field is needed, while the two room method requires two sound fields. This method is also considered to be more accurate since it does not need corrections for the surface area of the structure and the absorption of the receiving room.

Because the sound field in the cylinder is considered to be a reverberant field, the incident sound intensity inside the cylinder can be calculated with the interior space-average sound pressure level results and the formula $I_{in} = \frac{P_{in}^2}{4\rho_0 c_0}$ can be used.

First, the background sound intensity inside the cylinder was calculated to make sure the results were reliable in the frequency range of interest. Figure 38 shows the result obtained for the background sound intensity inside the cylinder.

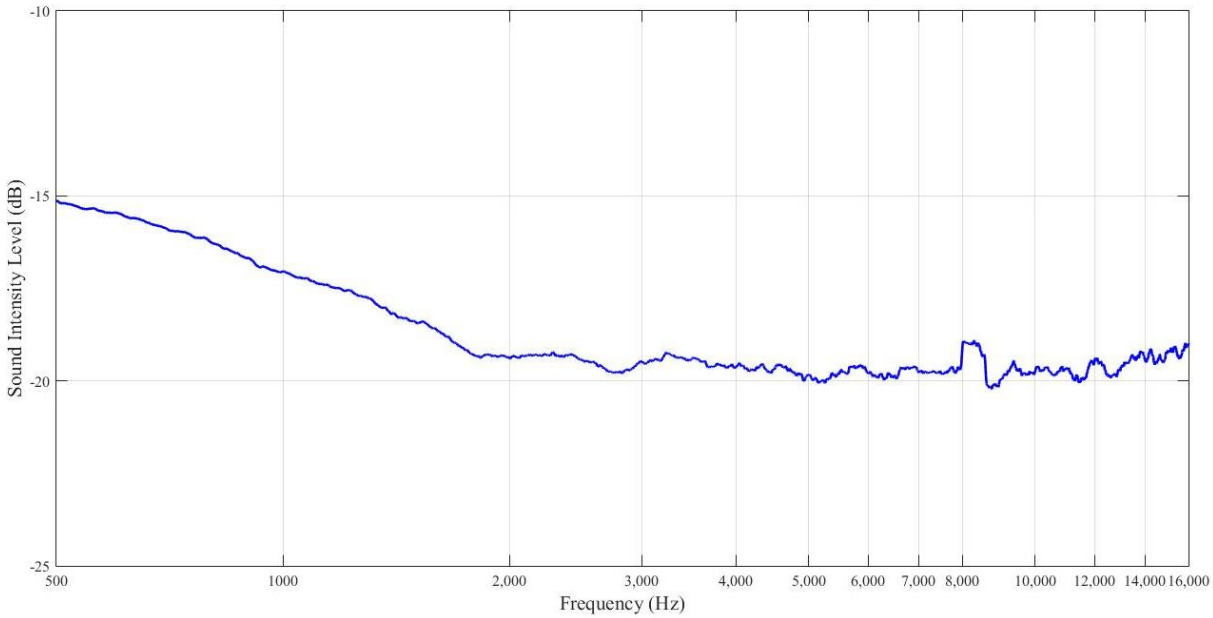

Figure 38: Background sound intensity level inside the cylinder.

The background sound intensity level in the receiving room was also measured by removing the noise sources in the room and using the sound intensity probe. The results are shown in Figure 39.

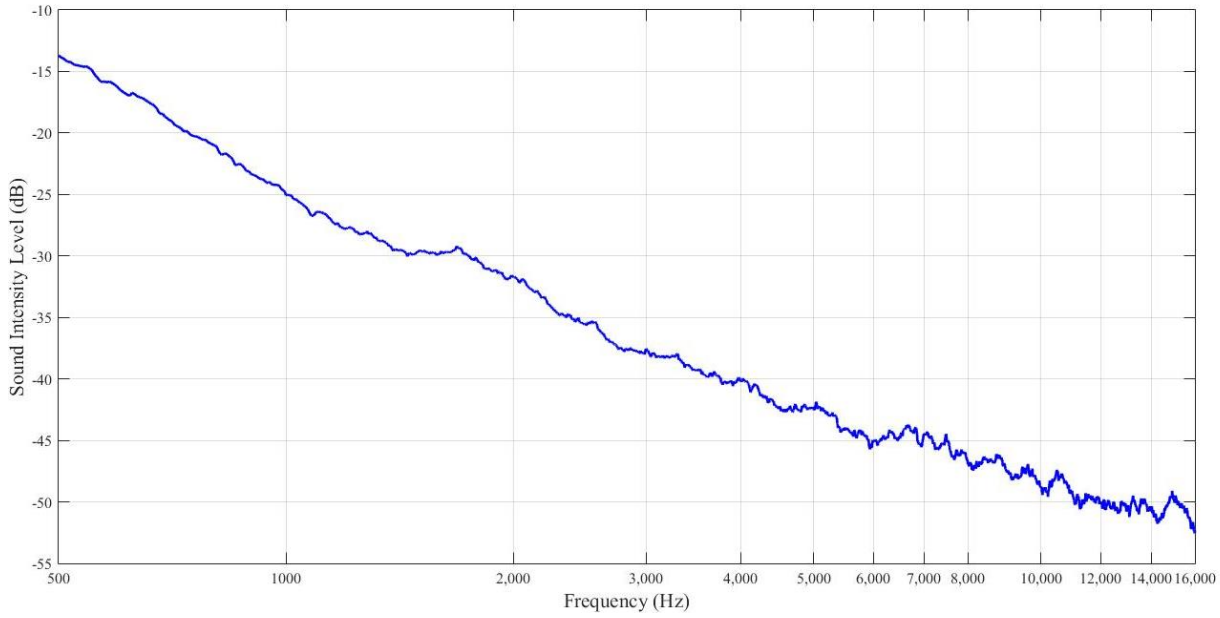

Figure 39: Background sound intensity level in the receiving room.

Then sound pressure level inside the cylinder with the loudspeakers on was measured and space-averaged for five different locations. The results obtained for intensity are plotted in Figure 40:

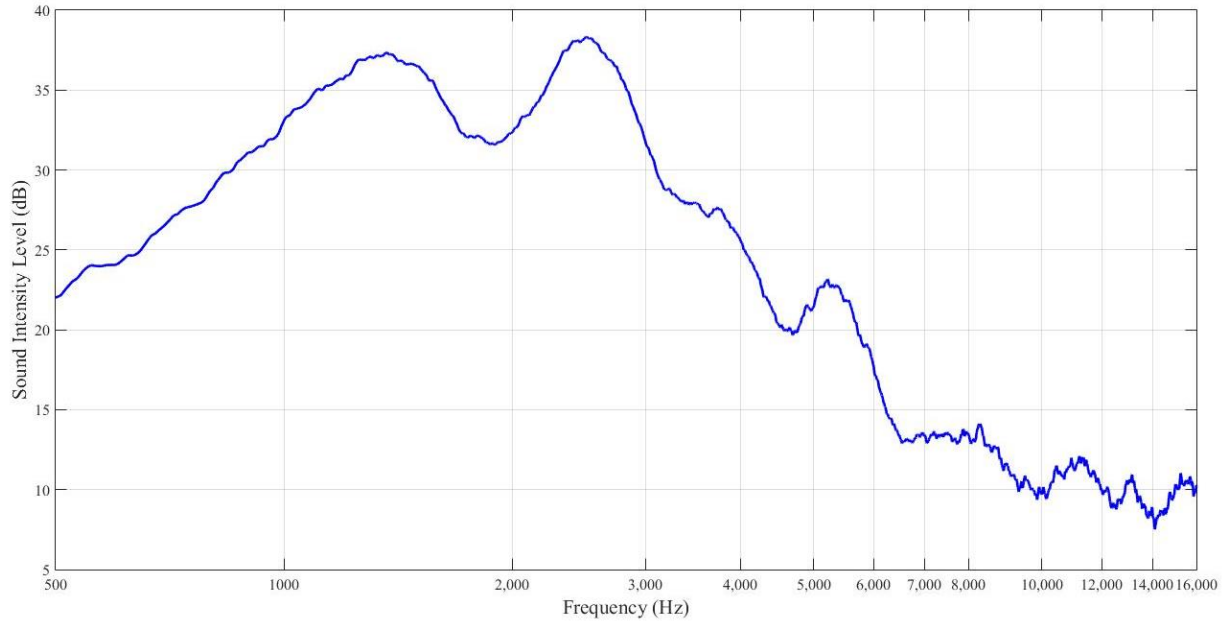

Figure 40: Sound intensity inside cylinder (calculated).

The results were compared to the background sound intensity level inside the cylinder, as shown in Figure 41 and it was concluded that the measurements inside the cylinder were reliable for the frequency range under investigation:

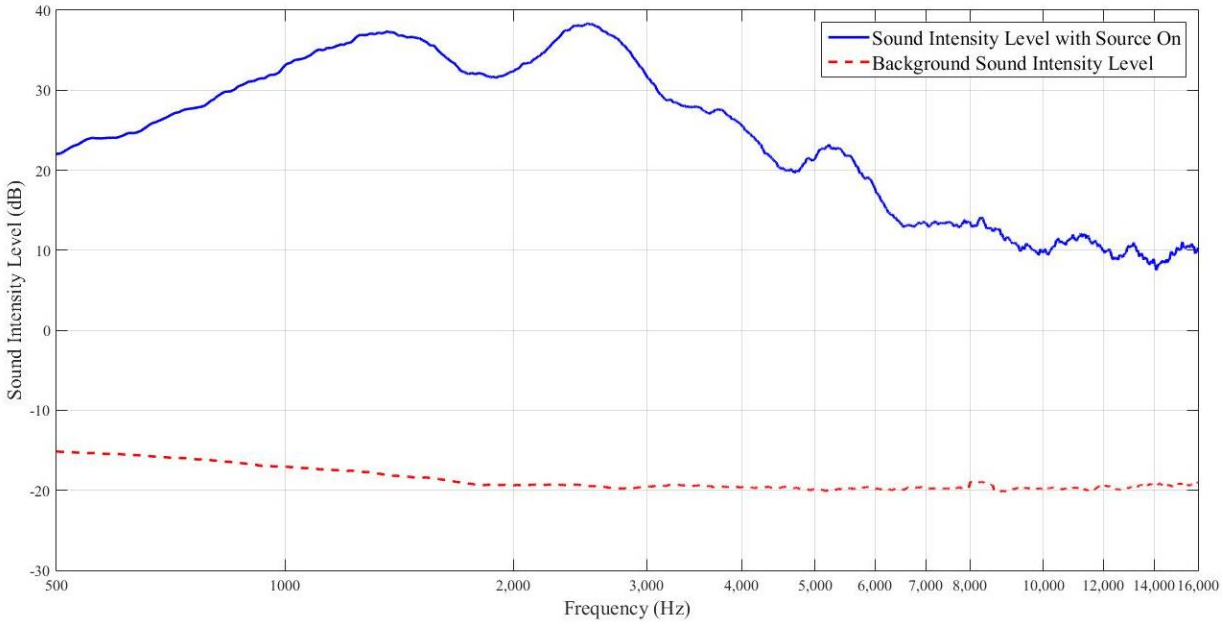

Figure 41: Background sound intensity level and sound intensity level with source on inside the cylinder.

Then, using the sound intensity probe, the sound intensity transmitted from outside the cylinder was measured following the procedure described in the appendix:

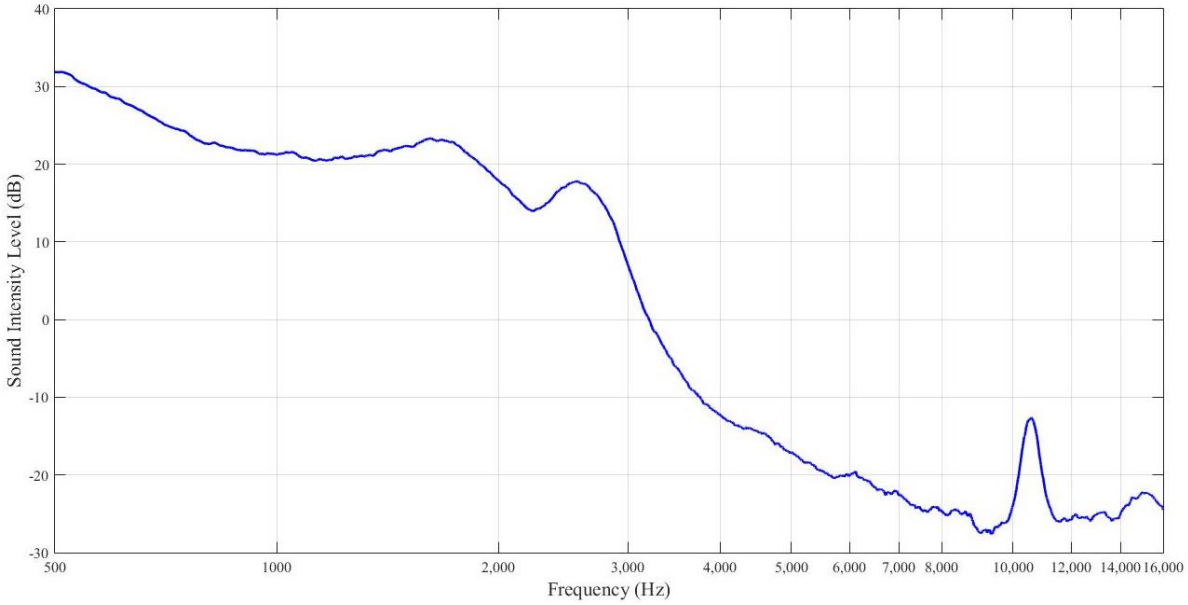

Figure 42: Measured sound intensity outside the cylinder.

The results were compared to the background sound intensity level in the receiving room, as shown in Figure 43 and it was concluded that the measurements in the receiving room were reliable as well for the frequency range under investigation:

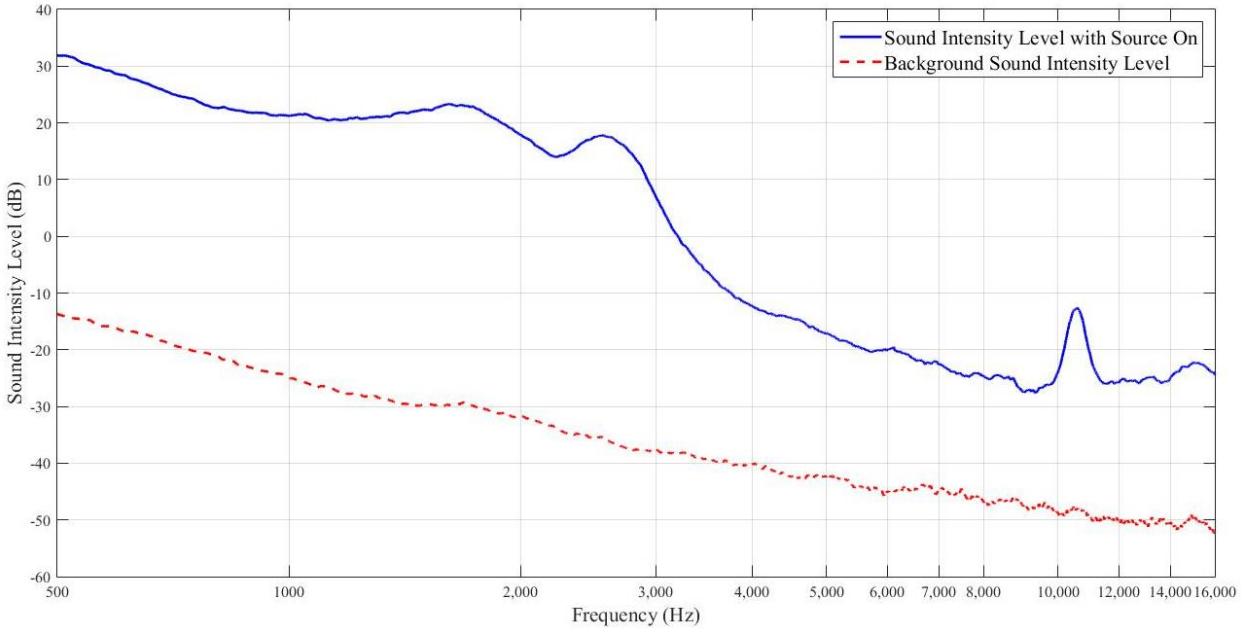

Figure 43: Background sound intensity level and sound intensity level with the loudspeakers on in the receiving room.

The intensity is much higher inside the cylinder since it is the source volume for this set of experiments. In the receiving room, a very pronounced dip can be seen at the critical frequency. Then transmission was calculated using the formula given previously:

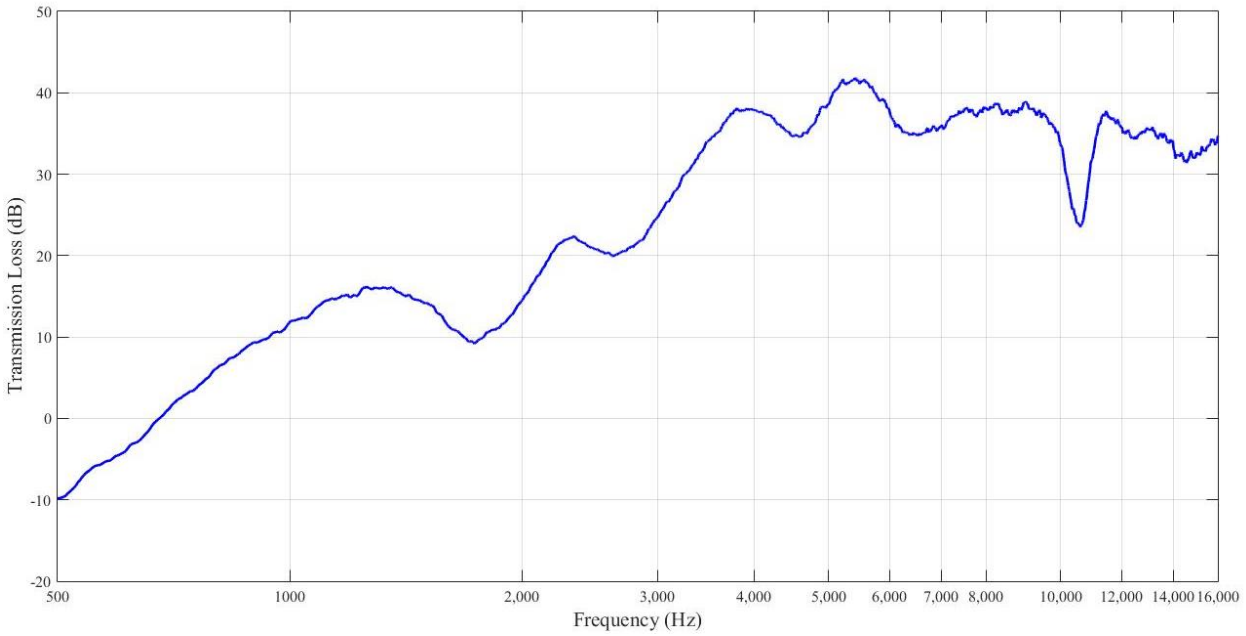

Figure 44: Transmission Loss using intensity probe.

At low frequency, the results do not seem to be reliable. The dips at the ring frequency and the critical frequency can be observed and the results seem reliable at higher frequencies (2,000 Hz to 12,000 Hz). Above 10,000 Hz, TL is not reliable since the intensity probe fails above about 10,000 Hz.

The sound pressure level measurements were also used to plot the experimental response of the cylinder relative to mass law. The acceleration of the cylinder was measured using an accelerometer placed at five different locations, these results were then averaged to obtain the space average acceleration of the panel. These results were used to plot the response of the panel relative to mass law:

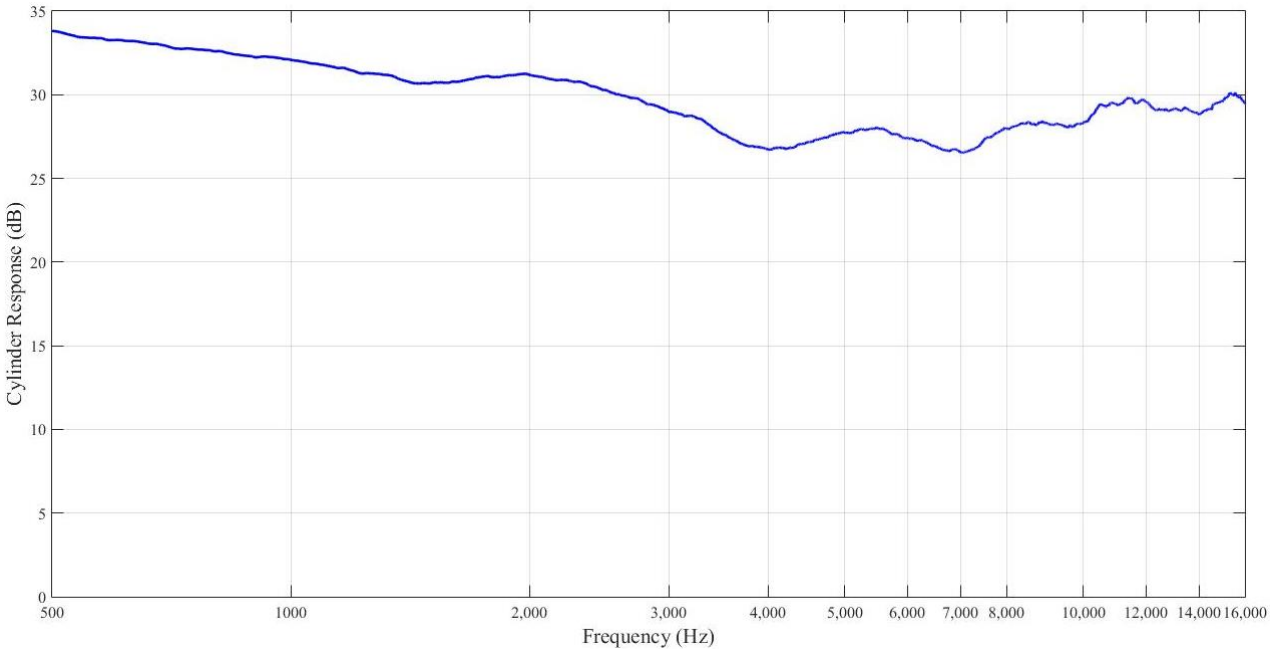

Figure 45: Experimental cylinder response relative to mass law.

Chapter 4: Comparison of the results:

` 4.1-Theoretical predictions and experimental results for the panel:

4.1.1-Theoretical predictions versus sound pressure level measurements:

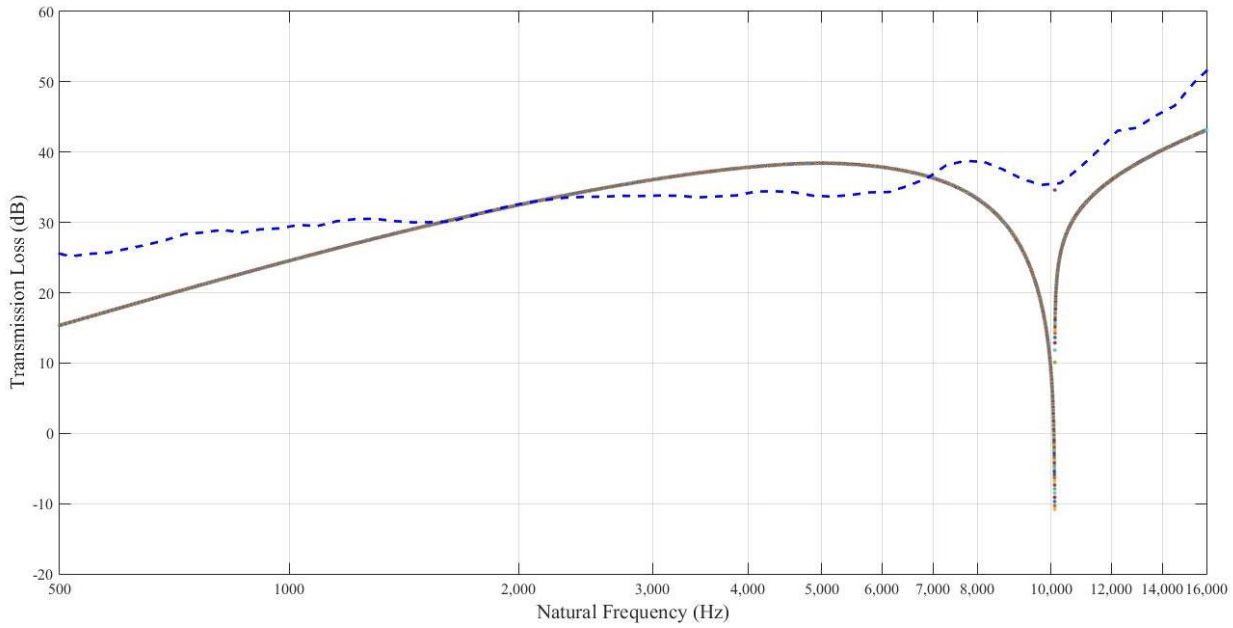

Figure 46: Theoretical panel transmission loss (solid line) and measured transmission loss (dashed line).

Figure 46 shows the theoretical SEA results obtained for transmission loss (TL) and those measured using sound pressure levels and the two room method. The critical frequency of 10,118 Hz predicted theoretically agrees fairly well with the TL measurements using sound pressure levels. The agreement of the measured results with the theoretical predictions is good at low frequencies. At high frequencies above 6,000 Hz and at frequencies in the critical frequency

range. These differences are caused by the interference of the background noise. The transmitted sound is not sufficiently above the background noise. The noise sources used were not powerful enough to produce a high enough sound pressure level in the receiving room at high frequencies. The agreement between the theory and measurements shows and the presence of a visible dip at the critical frequency. This gives confidence in the accuracy of SEA. The dip that can be observed at the critical frequency is more pronounced in the sound transmission loss predictions is calculated than it is in the measured sound transmission using this first method. The reason for that might be the difficulty in the measurements since the two room method requires creating a diffuse sound field and measuring the reverberation time of the room which was difficult.

4.1.2-Theoretical predictions versus sound intensity measurements:

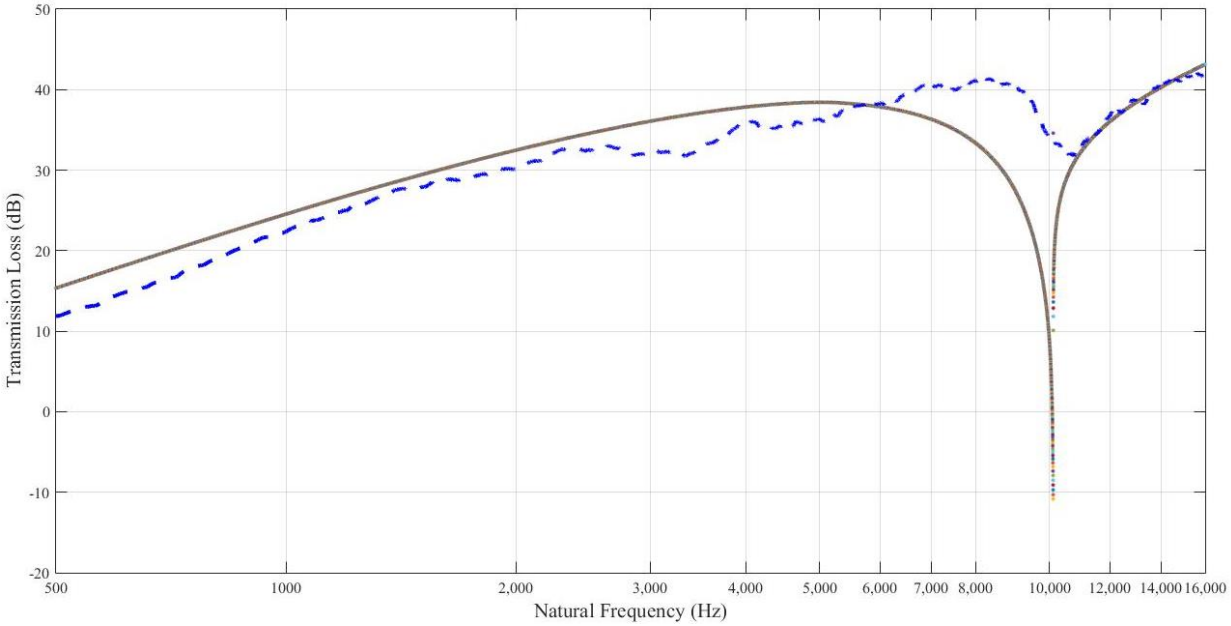

Figure 47: Theoretical panel transmission loss (solid line) vs transmission loss using sound intensity (dashed line).

Figure 47 shows the results obtained for transmission loss SEA predictions and measurements using the sound intensity probe. The critical frequency of 10,118 Hz predicted theoretically agrees reasonably well with the measurements of TL using sound intensity. At all frequencies, the sound intensity probe method and the theoretical predictions results are in good agreement (difference of around 2 dB). This proves that the experimental method gives accurate results but also the predictions of SEA are reliable. The dip that can be observed at the critical frequency is more pronounced when sound transmission is calculated than it is when sound transmission is experimentally determined using the intensity method. The assumptions used for this experimental method concerning the sound field for the source room to calculate the intensity incident on the panel proved to give accurate results.

4.1.3-Comparison of all the results for the panel:

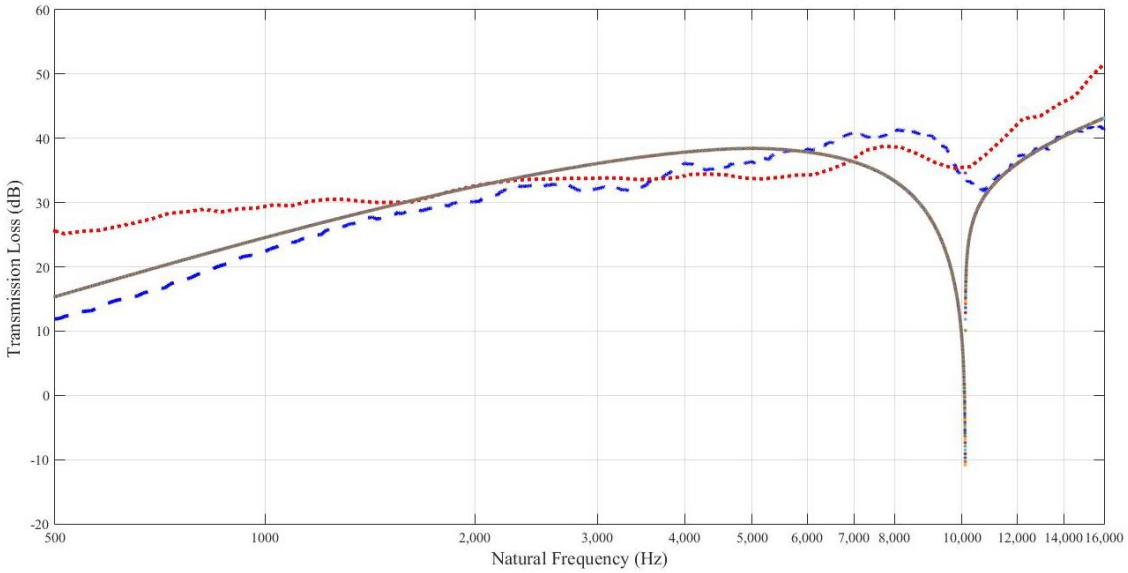

Figure 48: Theoretical panel transmission loss (solid line) vs transmission loss using sound pressure levels (dashed line) vs transmission loss using sound intensity levels (dotted line).

The theoretical SEA results and the results obtained using both of the experimental methods provided convincing results in the frequency range under consideration. The dip can be seen at the critical frequency and coincides for all methods used (approximately 10,118Hz). The dip is more pronounced for the sound intensity method. Using the sound intensity method however, seems to provide results that are in closer agreement with the theoretical SEA predictions. This was to be expected and can be explained by the fact that the intensity method is much easier to implement than the transmission suite method. Only one reverberation room is needed to use the sound intensity method and there is no need to measure the reverberation time of the reception room. Despite the difficulty of the implementation of the intensity method, it is interesting to see that the transmission loss obtained in close agreement with the sound intensity method counterpart.

It is also interesting to compare these results to the predictions of "mass law" theory which neglects the panel damping and stiffness and assumes the structure to be an infinite membrane and therefore doesn't predict the dip at the coincidence frequency. It can be noticed that below and above the critical frequency, the panel's response, whether it is calculated or measured agrees with "mass law" theory as it follows a slope of 6 dB per doubling of frequency. At the critical frequency however, the so-called "mass law' theory fails. This is shown in figure 49.

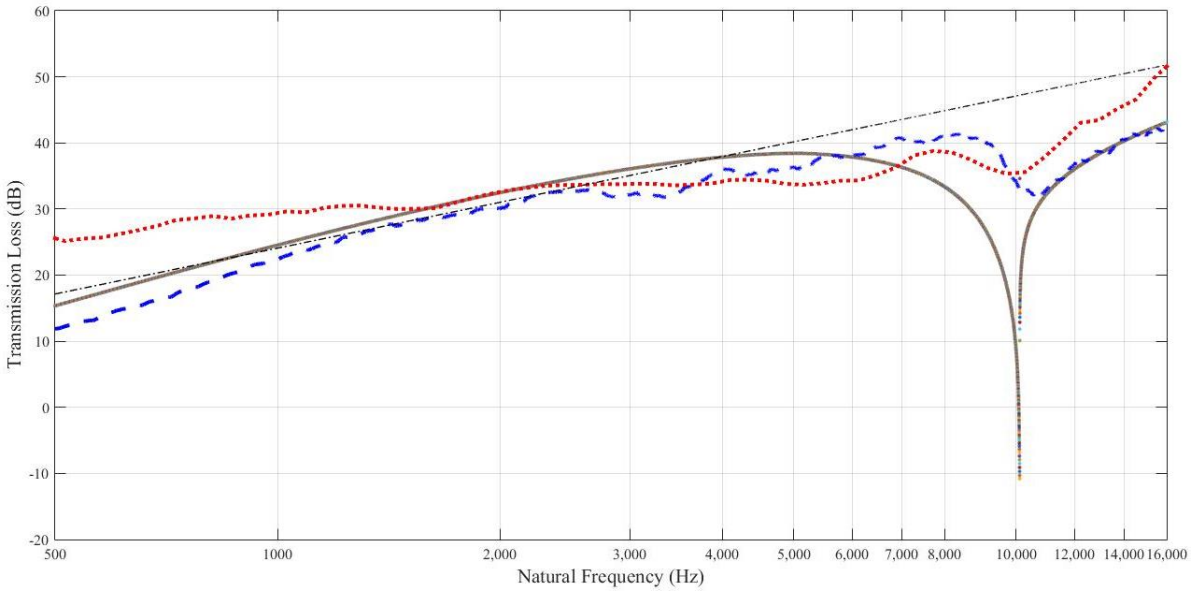

Figure 49: Theoretical panel transmission loss (line), panel transmission loss using sound pressure (dashes), panel transmission loss using sound intensity (dots) and 6 dB slope.

4.2-Theoretical predictions and experimental results for the cylinder:

4.2.1-Theoretical predictions versus sound pressure level measurements:

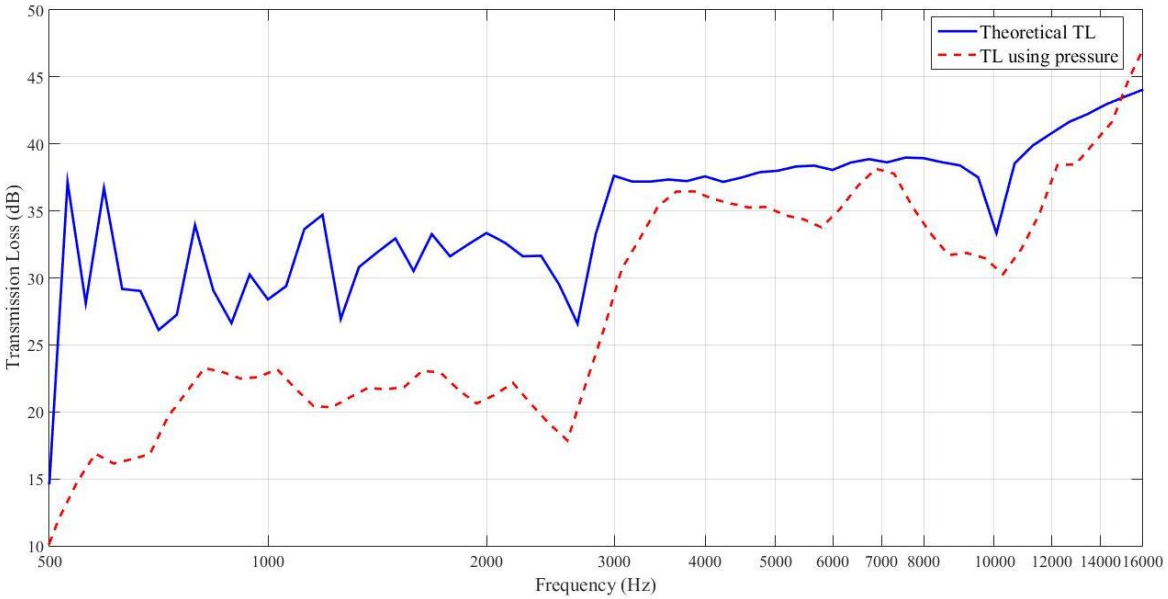

Figure 50: Theoretical cylinder transmission loss vs transmission loss using sound pressure levels.

Figure 50 shows the results obtained for the transmission loss of the cylinder using the transmission suite method and using theoretical SEA calculations. At low frequencies, the agreement between the theory and the transmission suite method is poor which can perhaps be explained by the fact that the interior volume of the cylinder does not have enough modes in the frequency range for coupling with the structural modes at low frequency. SEA is not very reliable at these frequencies because the assumptions made are not valid. The two dips at the ring and critical frequencies of the cylinder can be seen to agree quite well with the theory and measurements. The theoretical ring frequency for the cylinder is 2,625 Hz and the critical frequency is 10,118 Hz. For high frequencies, the agreement between the experimental method and the theory is better.

4.2.2-Theoretical predictions versus sound intensity measurements:

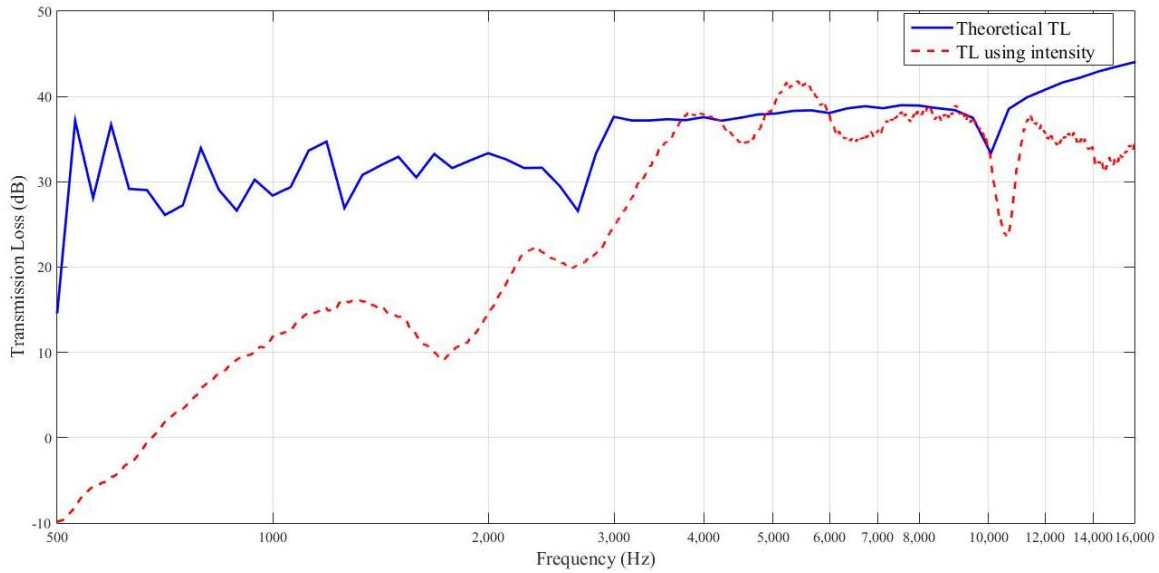

Figure 51: Theoretical cylinder transmission loss vs transmission loss using sound intensity levels.

Figure 51 shows the results obtained for the transmission loss of the cylinder using the sound intensity method and using theoretical SEA calculations. At low frequencies, the theoretical predictions and the experimental method do not agree well in magnitude, which may be explained by difficulties in creating a diffuse sound field inside the cylinder at these frequencies, the assumption $I_{in} = \frac{p_{in}^2}{4\rho_0 c_0}$ is not valid for the sound intensity in the source volume.

The two dips at the ring and critical frequencies of the cylinder can be seen with the theory and experiment and coincide. Then for higher frequencies, the sound intensity results do not seem to agree well with the theory which can be explained by the fact that the loudspeaker sources are not as powerful at higher frequencies which compromises the sound intensity measurements. The sound intensity probe also fails at high frequency.

4.2.3-Comparison of all the results for the cylinder:

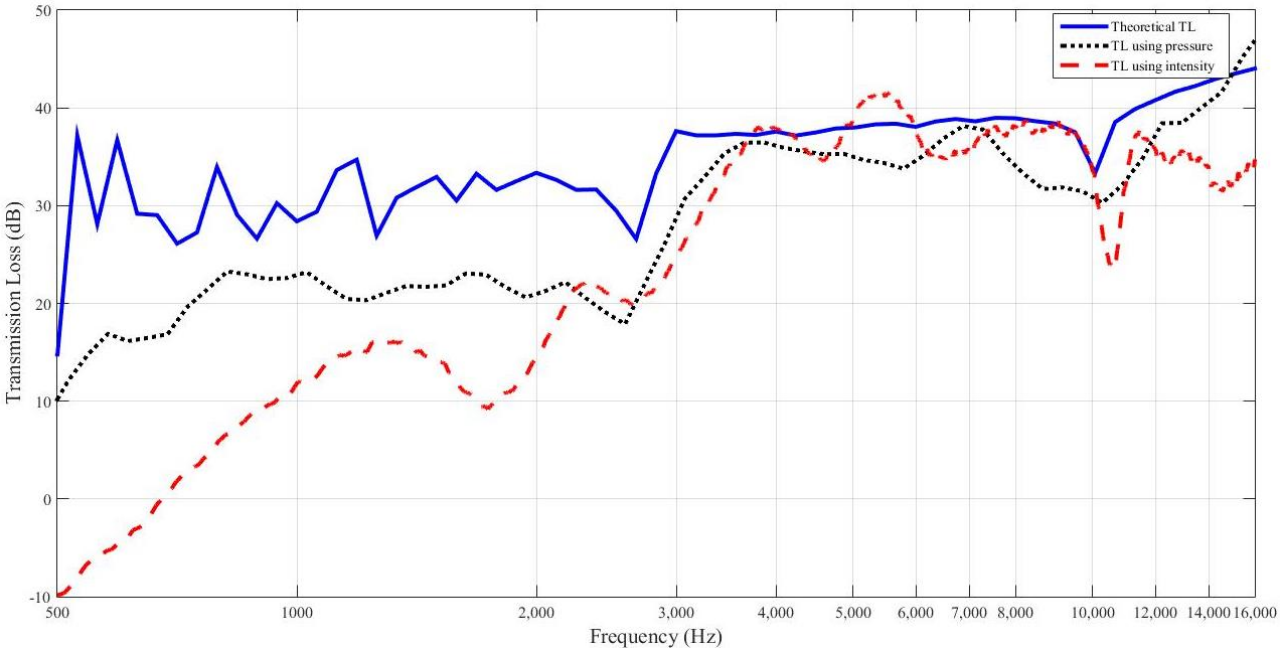

Figure 52: Theoretical cylinder transmission loss vs transmission loss using sound pressure vs transmission loss using sound intensity.

At low frequencies, the agreement in magnitude between the SEA theory and measurements is very poor [34]. However, it is safe to trust the two room method rather than the computational method or the sound intensity method because the assumptions made for both the SEA and the sound intensity calculation are not applicable in low frequencies. The ring frequency is apparent in all three results (approximately 2,625 Hz). The agreement is good in the region between the ring frequency and the crtitical frequency, where there is only a 3 dB difference between the three results. Finally, at high frequencies, the theory and the two room method seem to give the best results. The sound pressure level measured in the reception was high enough above the background sound pressure level to produce correct measurements.

However it was not the case for the sound intensity measurements since the sound intensity probe fails at high frequency.

4.3-Comparison between the panel behavior and the cylinder behavior:

4.3.1- Theoretical results:

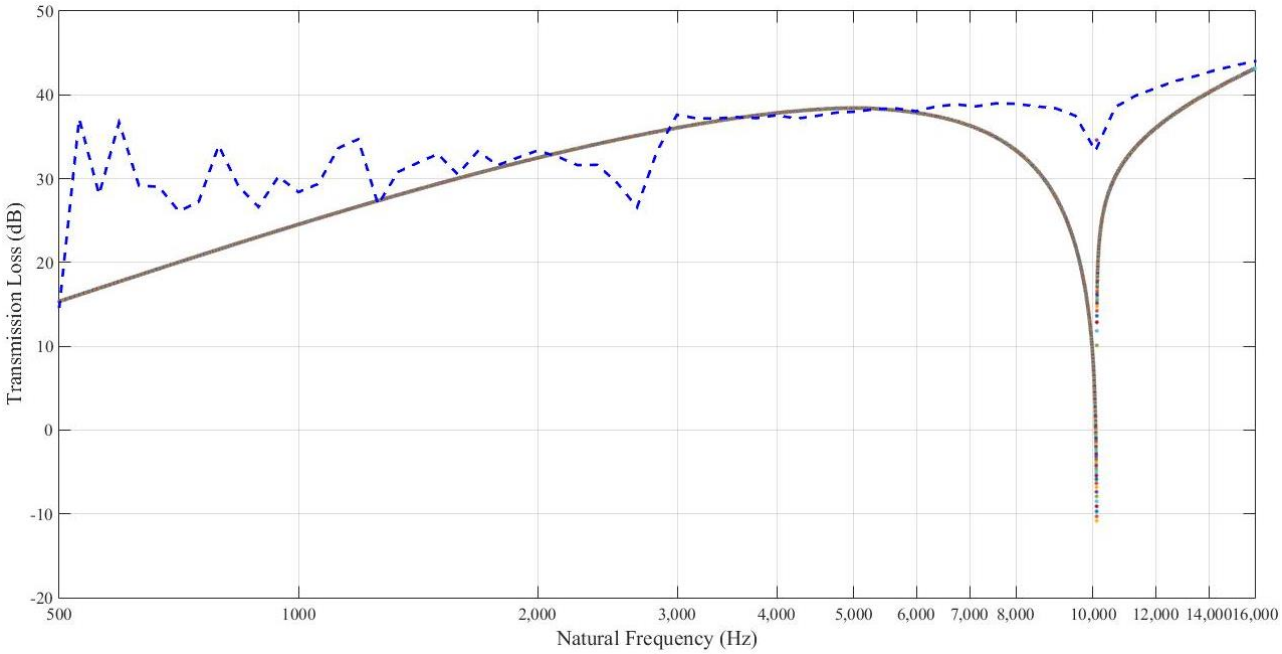

Figure 53: Theoretical cylinder transmission loss (dotted line) vs theoretical panel transmission loss (solid line).

As Figure 53 shows, the theoretical sound transmission loss obtained for both the cylinder and the panel have the similar amplitudes and follow a 6 dB per doubling of frequency slope except in the critical frequency region for the panel and the ring frequency region and the critical frequency region for the cylinder. Since the two structures studied in this project are made with the same metal material and have the same thickness, it is expected that their behavior

will be similar. The ring frequency being a geometrical property of the cylinder, it is also seen that it does not appear for the panel. At low frequency, the theoretical assumptions made for the cylinder are not the same as for the panel, which explains the difference between the sound transmission loss obtained for the cylinder and for the panel at these frequencies.

4.3.2- Results using the two room method and the sound intensity method:

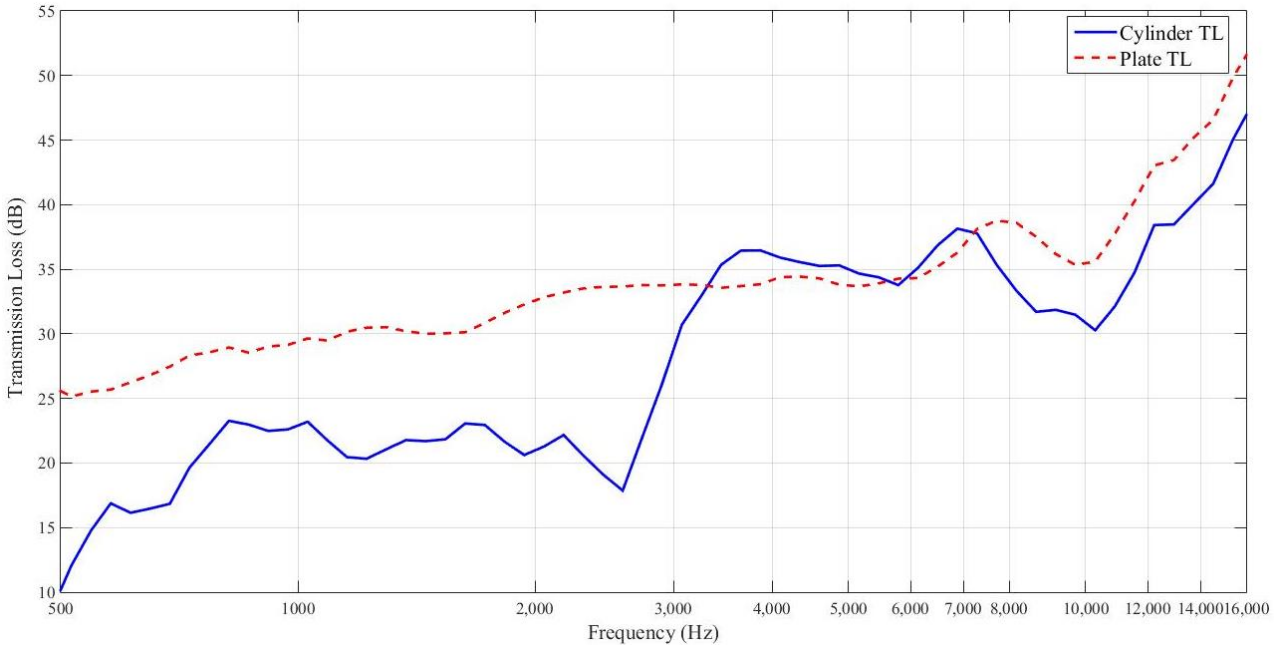

Figure 54: Measurements of the cylinder transmission loss using sound pressure vs panel measured transmission loss using sound pressure.

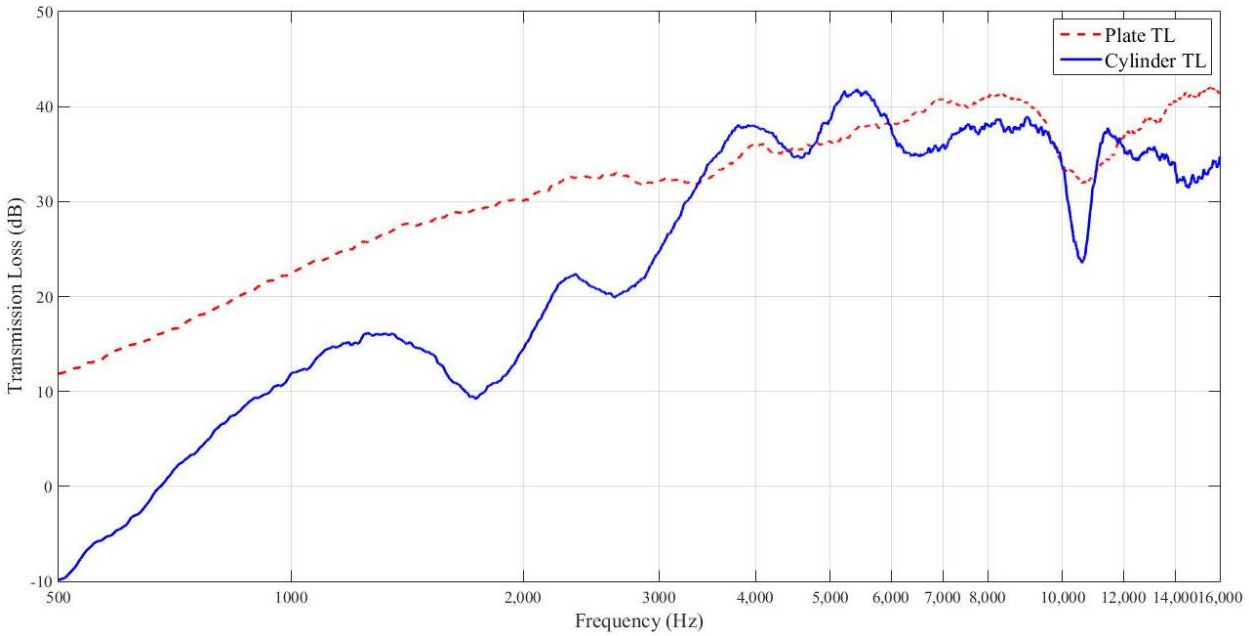

Figure 55: Measurements of the cylinder transmission loss using sound intensity vs measured panel transmission loss using sound intensity.

The results show that the critical frequency coincided for the two structures (10,118 Hz) for both experimental methods. The best agreement is obtained at frequencies higher than the cylinder's ring frequency. It is interesting to notice that the transmission suite method gives better results for the panel than it does for the cylinder, as also shown on Figure 54. This can be explained by the fact that for the experiments on the panel, two reverberant rooms were used for the investigation, which made the sound pressure level calculations more accurate. For the cylinder, however, the source room was the interior of the cylinder where the assumptions of a free field do not hold at low frequencies. The sound intensity method gives better results at frequencies higher than the ring frequency and lower than 12,000 Hz for the cylinder but gives good results for the whole frequency range for the panel, as shown in Figure 55. Overall, the sound intensity method seems to be the best suited for this study.

4.4- Panel and cylinder response relative to mass law:

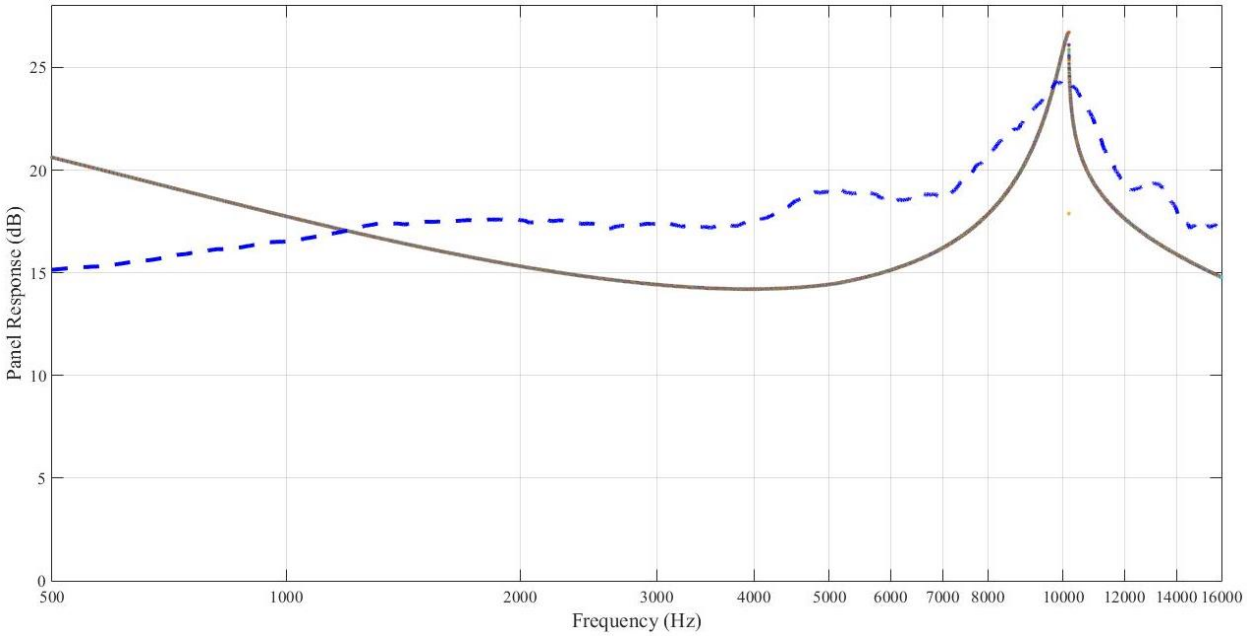

Figure 56: Theoretical panel response relative to mass law (line) vs experimental panel response relative to mass law (dashes).

As Figure 56 shows, the panel response relative to mass law using theory is in close agreement with to the experimental findings with a maximum difference of 2 dB to 3 dB at any frequency. A peak is noticeable at the critical frequency of the panel (10,118 Hz) using both methods.

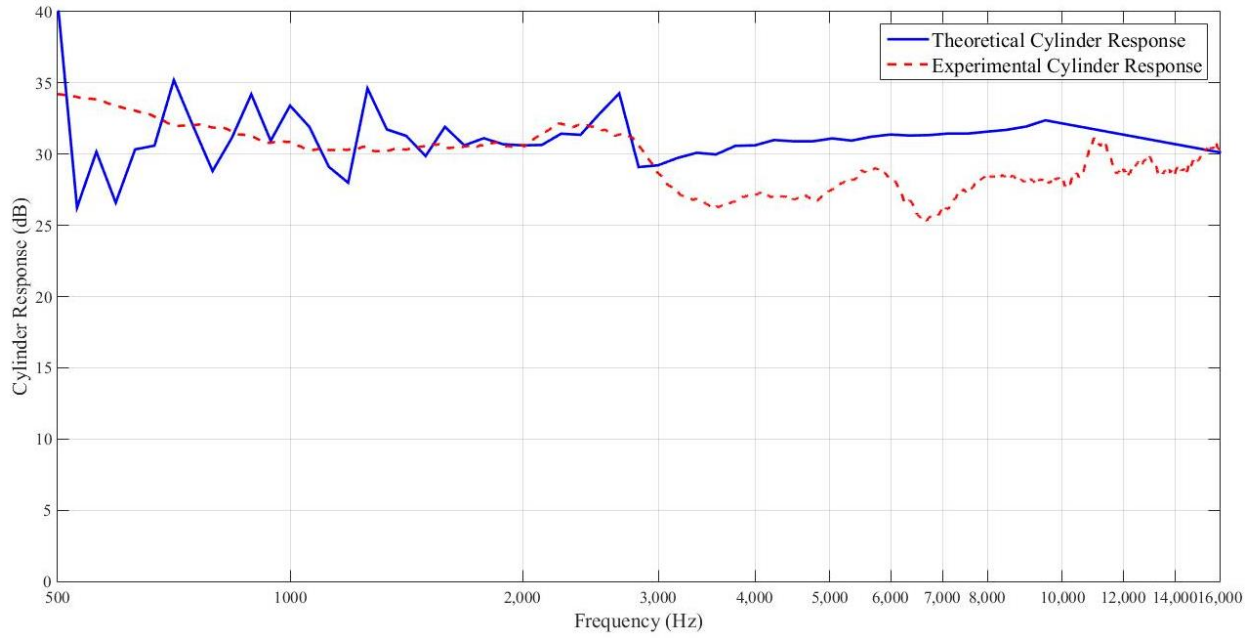

Figure 57: Theoretical cylinder response relative to mass law (line) vs experimental cylinder response relative to mass law (dashes).

From Figure 57, it can be noted that the agreement between the theory and the experiment is not as good as for the panel, although the maximum difference between the experiment and theory is of 4 dB at any frequency. This may be due to the structural behavior of the cylinder at lower frequency. A peak is present at the ring frequency, and above this frequency, the cylinder seems to behave similarly to the panel.

Chapter 5: Conclusion

The results obtained using the theory behind sound transmission through a flat panel were compared to the experimental results obtained using the two room method and the sound intensity method. This comparison showed that the sound intensity method gave more reliable results than the two room method. This can be explained by the difficulty of the setup for this method, the difficulty to measure the reverberation time of the room and the interference of the background noise with the measurements at high frequency. The sound intensity method however, gave results that were very similar to the theoretical results. The method was also easier to implement but failed at higher frequencies as well. The response of the panel relative to "mass law" was also investigated theoretically and experimentally through measuring the acceleration of the panel.

The theoretical and computational part for the cylinder was more complicated than the one used for the panel; the results, however, were convincing. The experimental implementation was easier for the cylinder as it was easier to produce enough sound only using the loud speakers. The two methods agreed relatively well with the theory, two dips could be seen at the ring and critical frequencies. As it was the case for the panel, the best results were obtained using the sound intensity method. The investigation proved the reliability of the SEA in the frequency range of interest and showed that the method should not be used for low frequencies as the assumptions made for higher frequencies were not valid in the low frequency range.

The flat panel and the cylindrical shell used for this study both have the same thickness and the same material properties. The shape was the only difference between the two structures. It was observed that the transmission loss for the two structures was following the prediction of "mass law" theory with a slope of 6 dB per doubling of frequencyexcept in the critical frequency region for the panel and at the ring frequency and the critical frequency region for the cylinder, where the experiments and the SEA did not agree with the so-called "mass law" theory.

Some difficulties were encountered during this project. The theoretical part as well as the programming part went rather well. The experimental part, on the other hand, did not go as smoothly. One of the notable difficulties encountered was with the setup itself. The experiment was conducted using a rather massive cylinder that had to be opened many times to change either the loudspeakers inside, add or remove fiberglass etc., which was a time consuming task. The thickness chosen for the panel made it difficult to have noise sources powerful enough in the sound transmission loss measurements. Measuring the reverberation time of the receiving room proved to be another difficult aspect of this project which affected the results obtained with the transmission suite method.

Despite the number of difficulties encountered during this project, it was a successful one as it gave interesting results for the sound transmission loss through two different structures. Further investigation of these structures can be done and can be useful to the aviation industry for instance.

References:

[1] Crocker M. *Handbook Of Noise And Vibration Control*. Hoboken, N.J. John Wiley. 2007.

[2] Liu Z, Yi C, The analysis of Vibro Acoustic Coupled Characteristics of Ball Mill Under Impact Excitation. *Modern Applied Science,* 2008.

[3] Petyt M. *Introduction to Finite Element Analysis*. Cambridge University Press. Cambridge, 1990.

[4] Lyon R, *Statistical Energy Analysis of Dynamical Systems: Theory and Application*. 1975.

[5] Smith, P. W. "Response and radiation of structural modes excited by sound." *The Journal of the Acoustical Society of America.* 1962.

[6] Lyon R, Maidanik G. Power Flow Between Linearly Coupled Oscillators. *The Journal of the Acoustical Society of America.* 1962.

[7] Crocker M. Recent Developments in Acoustics and Vibration. *International Congress on Sound and Vibration.* 1997

[8] Crocker M, Bhattacharya M, Price A J. Sound and Vibration Transmission Through Panels and Tie Beams Using Statistical Energy Analysis. *Journal of Sound and Vibration.* 1969.

[9] Utley W A, Mulholland K A J. Measurement of transmission loss using vibration transducers. *Journal of Sound and Vibration.* 1967.

[10] Kinsler E, Austin R F, Coppens A B, Sanders. *Fundamentals of Acoustics.* John Wiley & Sons. 1982.

[11] transmission suite method

[12] Fahy F J. *Sound Intensity*. 2nd Edition. E & FN Spon London. 1995.

[13] Pascal. Mesure de l'intensite active et reactive dans differents champs acoustiques. CETIM, Senlis. 1981.

[14] Lyon R, DeJong R. *Theory And Application Of Statistical Energy Analysis*. Boston:

Butterworth-Heinemann; 1995.

[15] Wallace CE Radiation Resistance of a Rectangular Panel. *Acoustical Society of America.*. 1972.

[16] Crocker M, Price A. Sound Transmission Using Statistical Energy Analysis. *Journal of Sound and Vibration*. 1969.

[17] Maidanik G. Response of Ribbed Panelsto Revereberant Acoustic Fields. *Acoustical Society of America.* 1962.

[18] Crocker M, The Response of Structures to Acoustic Excitation and the Transmission of Sound and Vibration. 1969

[19] Leissa A W. Vibration of Shells. NASA SP-288. 1975.

[20] Soedel W. *Vibration of Shells and Plates*. Marcel Dekker, Inc. 1981

[21] Koval L R. Effects of Cavity Resonances on Sound Transmission Into a Thin Cylindrical Shell. *Journal of Sound and Vibration*. 1978.

[22] Donnel L H. A Discussion of Thin Shell Theory. *Congress of Applied Mechanics*. 1938.

[23] Donnell L H. Stability of Thin Wall Tubed Under Torsion. NASA Report No 479. 1933.

[24] Mushtari K M. Certain Generalizations of the Theory of Thin Shells. Vol II, No 8. 1938.

[25] Wang, Y. Transmission of sound through a cylindrical shell and a light aircraft fuselage. 1982.

[26] Yu Y Y. Free Vibration of Thin Cyindrical Shells Having Finite Lengths with Freely Supported and Clamped Edges. *Journal of Applied Mechanics*. 1955.

[27] Soedel W. A New Frequency Formula for Closed Circular Cylindrical Shells for for a Large Variety of Boundary Counditions. *Journal of Sound and Vibration*. 1980.

[28] Manning J. Radiation Properties of Cylindrical Shells. *The Journal of the Acoustical Society of America*. 1964.

[29] Szechenyi E. Modal Densities and Radiation Efficiencies of Unstiffened Cylinders Using Statistical Methods. *Journal of Sound and Vibration.* 1971

[30] Wang Y, Crocker M, Raju P K. Theoretical and Experimental Evaluation of Transmission Loss of Cylinders. *AIAA Journal.* 1981.

[31] http://www.bksv.com/

[32] Wesley O. An Empirical and Computational Investigation into the Acoustical Environment at the Launch of a Space Vehicle. 2013.

[33] Farshidianfar A, Farshidianfar M H, Crocker M, Wesley O. Vibration Analysis of Long cylindrical Shells Using Acoustical Excitation. *Journal of Sound and Vibration*. 2011.

[34] Paquin J. Ametric for Comparing Acoustic Transmission Loss Curves. *Naval Research Laboratory*. Code 7180.

[35] Acoustics- Meaurement of Sound Insulation in Buildings and of Buinding Elements Using Sound Intensity. ISO 15186-1.

[36] Chung J Y, Pope J. Practical Measurement of Acoustic Intensity—The Two Microphone Cross-Spectral Method. Fluid Dynamics Research Department. General Motors Research Laboratories.

[37] Acoustics- Determination of Sound Power Levels of Noise Sources Using Sound Intensity. Part 2: Measurement by Scanning. ISO 9142-2

Appendix: 1 Matlab programs

```
% Program for computing the transmission loss for the panel using SEA:
% Panel Constants
hp = 0.00127;     % thickness of panel m
lp = 0.609;       % length of panel m
Lp = 1.04;        % width of panel m
Ap = lp*Lp;       % Area of panel m*m
Cp = 5800;        % speed of sound in panel m/s
Mp = 6.32;        % mass of the panel kg
P  = 2*(lp+Lp);   % perimeter of the panel m
fc = 10118;       % critical frequency of panel Hz
lambda_c = cp/fc; % wavelength m
wc = 2*pi*fc;     % angular frequency rad
% Other constants
c = 343;          % speed of sound m/c
rho = 1.21;       % density of air kg/m3
A = 16.47;        % Area of the room m*m
V = 68.5;         % volume of the room m3
fmax = 16000;     % maximum frequency Hz
RT= 0.161*V/A;    % Reverberation Time  s
nuint = 0.02;     % Internal loss factor
% syms w a(w) lambda(w) g1(w) g2(w) R(w) nr(w) nu13(w) n1(w) n2(w) n3(w) nu3(w) NR(w)
Tl(w) T(w)
```

```
for f=0:1:fmax
   alpha = sqrt(f/fc);
   lambda = cp/f;
   w = 2*pi*f;
   n1 = V*w^2/(2*pi^2*c^3);
   n2 = Ap*fc/(2*c^2);
   n3 = n1;
   nu3 = 2*2/(f*RT);
    if f < 0.5*fc
       g1=(4/pi^4)*(1-2*alpha^2)/(alpha*((1-alpha^2)^0.5));
    else
       g1=0;
    end
    g2 = ((2*pi)^(-2))*(((1-alpha^2)*log((1+alpha)/(1-alpha)))+2*alpha)/((1-alpha^2)^1.5);
if f < fc
   R =
Ap*rho*c*((lambda_c*lambda*2*(f/fc)*g1/Ap)+(P*lambda_c*g2/Ap));
elseif f == fc
   R = Ap*rho*c*((lp/lambda_c)^(-0.5)+(Lp/lambda_c)^0.5);
elseif f > fc
   R = Ap*rho*c*(1-(fc/f))^(-0.5);
end
nr = R/(w*Mp);
T = 10*log10((w^2)*Mp^2/(4*rho^2*c^2));
```

```
nu13 = Ap*c*exp((-T/10)*(log(2)+log(5)))/(4*V*w);
NR=-10*log10(nu13+(nr^2*(n2/n1)/(nuint+2*nr)))+10*log10(nu3+(n1*nu13/n3)+(n2*nr/n3))
TL= NR+10*log10(Ap*c*RT/(24*V*log(10)));
plot (f,TL,'.','markersize',8)
hold on
end
% Program for computing the transmission loss for the Cylinder using SEA:
function [TL,f_o] = wang_SEA
% close all
% clear all
% clc
C_o = 343;          % Speed of sound in air m/s
L = 2.0066;         % Length of the cylinder
rho_o = 1.21;       % kg/m3 Noise Control
R = 0.3048;         % Radius m
S = 2.*pi*R*L;      % surface area m2
h = 0.00127;        % thickness m (0.050")
rho = 7850;         % Steel density kg/m3
E = 2E11;           % Steel Young's Modulus
Poisson = 0.28;     % Steel Poisson's Ratio
m_s = rho*h;
% f_r = 2625.0;
% f_c = 10540.6;
f_r = (1./(2.*pi.*R)).*((E./rho).^0.5);  % Wang 2635.6
```

```
f_c = (C_o.*C_o.*(12.^(0.5))./(4.*pi.*pi.*f_r.*R.*h); % 10,118
% w_c =  2.*pi.*f_c;
%%%%%%% Bandwidth analysis %%%%%%%
% From function "Acoustic_Loads_subroutines_2_13"
frequency_maximun = 20000;
frequency_minimum = 20;
iii=1; ii=0;
frequency_center = 1000;
frequency_octave_size = 12;
bandwidth_ratio = 2.^(1/frequency_octave_size);
Freqc = zeros(1,9);
Freqc(1,1) = frequency_center;
while Freqc(1,1)>=frequency_minimum
   Freqc(1,1) = Freqc(1,1)/bandwidth_ratio;
end
while Freqc(1,iii)<=frequency_maximun
   iii=iii+1;
   Freqc(1,iii) = bandwidth_ratio*Freqc(1,iii-1);
end
deltafc = zeros(1,(iii-1));
while ii<iii
   ii=ii+1;
   deltafc(1,ii) = Freqc(1,ii).*((bandwidth_ratio- 1)./(bandwidth_ratio).^(1/2));
end
```

```
frequency_band_width = deltafc'; % The band width of each 1/N octaves section based on Freqc.

frequency_band_center = Freqc' ; % This is the center frequency of the bandwidth divided into
1/N octaves.

% Freq_number or Freq were the lower frequency of a spectrum bandwidth

% frequency_band_width = 10;

% frequency_band_center =
[frequency_minimum:frequency_band_width:frequency_maximun]';

frequency_band = zeros(length(frequency_band_center),5);

frequency_band(:,2) = frequency_band_center;

frequency_band(:,1) = frequency_band_center - frequency_band_width./2 ;

frequency_band(:,3) = frequency_band_center + frequency_band_width./2 ;

w_frequency_band = 2.*pi.*frequency_band;

v_frequency_band = w_frequency_band/(2.*pi.*f_r);

%.....................................................................

f_o = frequency_band(:,2);

w_o = 2.*pi.*f_o;

f_o_length = length(f_o);

v_o_array = w_o/(2.*pi.*f_r);

k_o_array = w_o./C_o;

m = 0:1:500;

n = 0:1:500;

m_length = length(m);

n_length = length(n);

k_temp = (h.*h.*R.*R./(12.*(1-Poisson.*Poisson))).^(0.25);

% ka_C = m+0.5;
```

```
% P_array = 1-2./(ka_C.*pi);
% k_a_array = (m.*pi./(L.*ka_C)).*k_temp;
k_c_array = (n./(R)).*k_temp;
k_a_array = (m.*pi./L).*k_temp;
v_mn = zeros(m_length,n_length);
E_rad_array = zeros(f_o_length,2);
D1=0;
E1=1;
v_frequency_band_above=0;
v_frequency_band_below=0;
for B1=1:m_length
   k_a=k_a_array(B1);
% P = P_array(B1);
% P1 = (1-Poission.*Poission)./(1-Poission.*Poission.*P);
% P2 = (1-Poission.*P.*P)./(P.*(1-Poission));
% k_a2 = k_a.*k_a;
%k_a4 = k_a2.*k_a2;
for C1=1:n_length
k_c = k_c_array(C1);
%k_c4 = k_c2.*k_c2;
%k_c2 = k_c.*k_c;
k_temp = (k_a.*k_a+k_c.*k_c).*(k_a.*k_a+k_c.*k_c);
v_mn(B1,C1) = sqrt(k_temp+k_a.*k_a.*k_a.*k_a./k_temp);
```

```
% v_mn(B1,C1) =
sqrt(k_a4+k_c4+2.*k_a2.*k_c2.*P+k_a4./(P1.*(k_a4+k_c4)+2.*k_a4.*k_c2.*P 2));

while D1==0

   if isnan(v_mn(B1,C1))

      v_frequency_band_below = v_frequency_band_below + 1;

      D1=1;

   elseif v_mn(B1,C1)<=v_frequency_band(1,1)

      v_frequency_band_below = v_frequency_band_below + 1;

        D1=1;

   elseif v_mn(B1,C1)>=v_frequency_band(f_o_length,3)

      v_frequency_band_above = v_frequency_band_above + 1;

      D1=1;

       elseif (v_mn(B1,C1)>=v_frequency_band(E1,1)) &&
(v_mn(B1,C1)<=v_frequency_band(E1,3))

           k_o = k_o_array(E1);

           v_frequency_band(E1,4) = v_frequency_band(E1,4) + 1;

           k_m = m(B1).*pi./L;

            k_n = n(C1).*pi./(2.*pi.*R);

           %k_o.*k_o

           %k_a.*k_a+k_c.*k_c

           k_check = (k_o.*k_o)>(k_m.*k_m+k_n.*k_n);

           v_frequency_band(E1,5) = v_frequency_band(E1,5) +  k_check;

           % acoustically fast

           ff = f_o(E1)./f_c;

           ff2 = (ff).^(0.5);
```

```
            kk = (k_a.*k_a+k_c.*k_c).^(0.5);
            piL = pi.*L.*((12.*(1-Poission.*Poission)).^(0.25));
            E_rad_temp = (((h.*R).^(0.5)).*(log(...
                (1+ff2)./(1-ff2)+(2.*ff2)./(1-ff)))))./(piL.*kk.*(1- ff2));
            E_rad_array(E1,1) = E_rad_array(E1,1) + E_rad_temp;
            % acoustically slow
        D1=1;
    elseif E1>f_o_length
        error('ERROR')
    else
        %nothing
    end
    E1=E1+1;
end
D1=0;
E1=1;
end
end
% total_number = 301*301
%  total_number_mn = v_frequency_band_below + v_frequency_band_above +
sum(v_frequency_band(:,4))
 n_w_o = v_frequency_band(:,4)./frequency_band_width;
%   hhhhh = figure;
%  axes1 = axes('Parent',hhhhh,...
```

```
%     'Position',[0.10 0.10 0.80 0.75],...
%     'XLim',[20 20000],...
%     'XScale','log',...
%     'GridLineStyle',':',...
%     'Box','on',...
%     'xtick',[10:10:90,100:100:900,1000:1000:9000,10000:10000:100000],...
%     'XTickLabel',{'10';';';';';';';';';'100';';';';';';';';';'
';'1000';';';';';';';';';';'10000';';';';';';';';';';'10000 0'});
%  line(frequency_band(:,2),n_w_o,'Color','r','LineStyle','- ','Parent',axes1,'LineWidth',0.5);
%  xlabel(axes1,'Frequency (Hz)','Color',[0,0,0],'FontSize',12)
%  ylabel(axes1,'Modal Density (Modes/Hz)','Color',[0,0,0],'FontSize',12)
 E_rad = zeros(f_o_length,1);
 E_rad_array(:,2) = v_frequency_band(:,5)./v_frequency_band(:,4);
 for F1=1:f_o_length
    test_F1 = real(E_rad_array(F1,2));
    if test_F1>=1
       % acoustically fast
         E_rad(F1) = 1;
    elseif (test_F1<1) && (test_F1>0)
       % acoustically fast and slow
        E_rad(F1) = test_F1;
    elseif (test_F1==0) || isnan(test_F1)
       % acoustically slow
         E_rad(F1) = real(E_rad_array(F1,1));
```

```
    else
    error('ERROR')
    end
end
E_mech = zeros(f_o_length,1);

for G1=1:f_o_length
    test_G1 = v_o_array(G1,1);
    if test_G1<=0.5
        E_mech(G1) = 0.01.*(1./(11.224489795918.*test_G1 + 12.612244897959)).*(f_r./f_c);
    elseif (test_G1>0.5) && (test_G1<=0.9)
        E_mech(G1) =  (5.5E-4).*(f_r./f_c);
    elseif (test_G1>0.9) && (test_G1<1.1)
         E_mech(G1) =  0;
    %0.00001.*(1./1.5).*(f_r./f_c);
    elseif test_G1>=1.1
         E_mech(G1) = -(5E-8).*f_o(G1)+0.001;
    else
        error('ERROR')
    end
end
R_rad = rho_o.*C_o.*E_rad.*S;
%  E_mech_old = -(5E-8).*f_o+0.001;
%  % % % E_mech = 0.0012;
```

```
R_mech = S.*m_s.*E_mech.*w_o;
%  figure
%  plot(v_o_array,E_mech)
%  test0 = (1./E_mech).*(f_r./f_c);
%  figure
%  plot(v_o_array,test0)
%  E_rad_plot = 10.*log10(E_rad);
%  for G1=1:f_o_length
%      if isfinite(E_rad_plot(G1))
% %  nothing
%      else
%          E_rad_plot(G1)=-60;
%      end
%  end
%
% figure
% plot(f_o,E_rad)
% Transmission of Sound Through a Cylindrical Shell and a Light Aircraft Fuselage
(Dissertation ) - Yiren Simon Wang - 1982
 TL_res =
10.*log10((w_o.*w_o.*m_s.*S.*S.*(2.*R_rad+R_mech))./(8.*pi.*pi.*C_o.*C_o.*n_w_o.*R_ra
d.*R_rad));
TL_nr = zeros(f_o_length,1);
TL = zeros(f_o_length,1);
 for A1=1:f_o_length
```

```
    v_o = v_o_array(A1,1);
    hR2 = (h/R).*(h/R);
    rho_C_o2 = rho_o.*rho_o.*C_o.*C_o;
    v_o_fr_fc2 = (v_o.*f_r./f_c).*(v_o.*f_r./f_c);
    v_o_fr_fc2_15 = (1-v_o_fr_fc2).^0.5;
    v_o_fr_fc2_12 = (1-v_o_fr_fc2).*(1-v_o_fr_fc2);
    if v_o<1
        TL_nr(A1) =(8.33.*log10((v_o.*v_o.*hR2.*E.*rho/(4.*rho_C_o2)) .* v_o_fr_fc2_12 + 2.3
)-3+20.*log10((pi./2).*asin((v_o.*v_o_fr_fc2_15)).^0.5));
        TL(A1) = 10*log10(TL_nr(A1))+TL_res(A1);
    elseif (v_o>=1.0) && (v_o<(f_c/f_r))
         TL_nr(A1) =( 8.33.*log10( (v_o.*v_o.*hR2.*E.*rho/(4.*rho_C_o2)).* v_o_fr_fc2_12 +
2.3 )-3);
            TL(A1) = 10*log10(TL_nr(A1))+TL_res(A1);
    elseif v_o>=(f_c/f_r)
        TL_nr(A1) =( 8.33.*log10( (v_o.*v_o.*hR2.*E.*rho/(4.*rho_C_o2)).* v_o_fr_fc2_12 + 2.3
)-3);


        TL(A1) = 10*log10(TL_nr(A1))+TL_res(A1);
    else
    error('ERROR')
    end
end
plot(f_o, TL)
xlabel(axes1,'Frequency (Hz)','Color',[0,0,0],'FontSize',12)
```

```
 ylabel(axes1,'Transmission Loss (dB)','Color',[0,0,0],'FontSize',12)
theta=linspace(0,2*pi);
ZZ = linspace(0,L);
XX = R.*cos(theta);
YY = R.*sin(theta);
XX = repmat(XX(:),1,size(ZZ,2));
YY = repmat(YY(:),1,size(ZZ,2));
ZZ = repmat(ZZ,size(XX,1),1);
%  TLS= zeros(size(ZZ));
%  for k=1:f_o_length
%   for i=1:size(ZZ)
%       for j=1:size(ZZ)
%       TLS(i,j)=TL(k);
%       end
%   C=TL.colors(size(ZZ));
%           figure
% surf(XX,YY,ZZ,C);
% getframe
%   end
 end
% surf(XX,YY,ZZ)
% hold on
% image(TLS,'CDataMapping','scaled')
%  while u<f_o_length
```

```
%     im=im(u+1);
%     C=im.Cdata;
%     figure
%     surface(XX,YY,ZZ,C)
%     u=u+1;
```

Appendix 2: Procedure for sound intensity measurements:

The measurements made using a sound intensity probe were performed following the international standard ISO 15186 Acoustics-Measurement of sound insulation in buildings and of building elements using sound intensity [35, 36, 37]. This appendix briefly explains the scope of this standard and its use during this study.

ISO 15186 is divided into 3 parts: Laboratory measurements, field measurements and laboratory measurements at low frequency. The first part of the standard was the most useful since the experiments conducted during this study were made in a laboratory and for a frequency range of 1000Hz to 16kHz. The sound intensity probe used for the experiments was a TYPE 3599 probe from B&K.

Figure 58: Sound intensity probe with microphones in the face to face arrangement.

ISO 15186 states that the calibration of the probe is a first step in conducting experiments. The probe was sent to the B&K company for calibration before the start of the experiments and then checked periodically using the calibrator provided by the company.

Figure 59: Sound intensity probe calibrator.

The test procedure was followed according to ISO 140 for the sound field generation and the measurement of the sound pressure level in the source room. The measurement of the average sound intensity level on the receiving side was conducted following the scanning procedure for the measurement surface. The probe was always held normal to the measurement surface while scanning and directed to measure the positive intensity outwards from the structure. The speed of scanning was kept constant. For the panel, the measurement surface was

the panel surface. The cylinder surface, however, was divided into 4 areas which were each scanned separately.

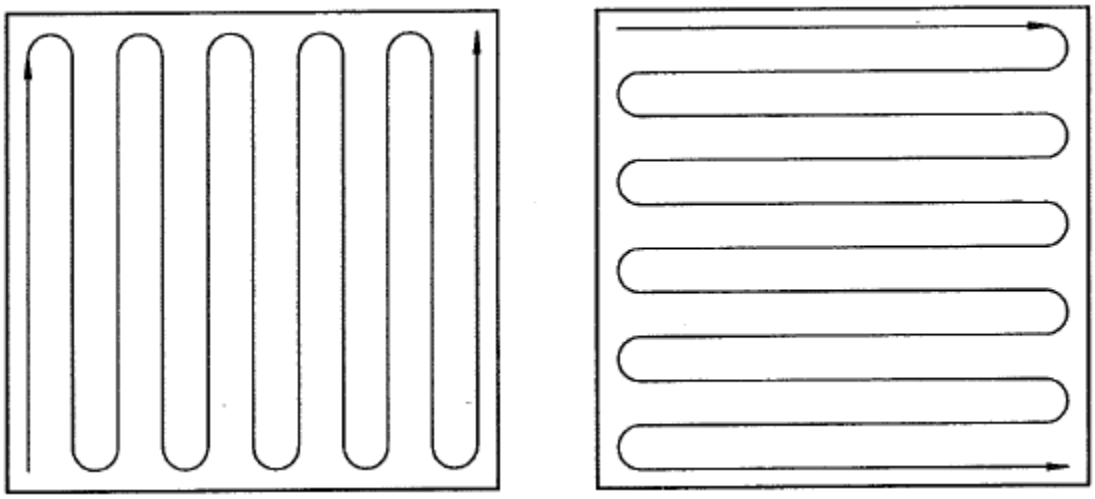

Figure 60: Scanning patterns.

The sound intensity uses a method known as the two-microphone method, which has been used and discussed by many engineers and scientists. Two configurations can be used for this technique; the microphones can be placed side-by-side or face-to-face with a spacer between them. The B&K sound intensity probe has its microphones placed face-to-face. In this configuration, the microphones must be phase matched, which makes this sound intensity probe difficult to calibrate. Parts of the sound intensity probe must be dissembled, to determine the phase and magnitude difference for measurements of the sound intensity with the microphones side-by-side.

With the loud speaker located inside the cylinder, the sound intensity in the receiving room was measured using both configurations to determine the sound intensity level.

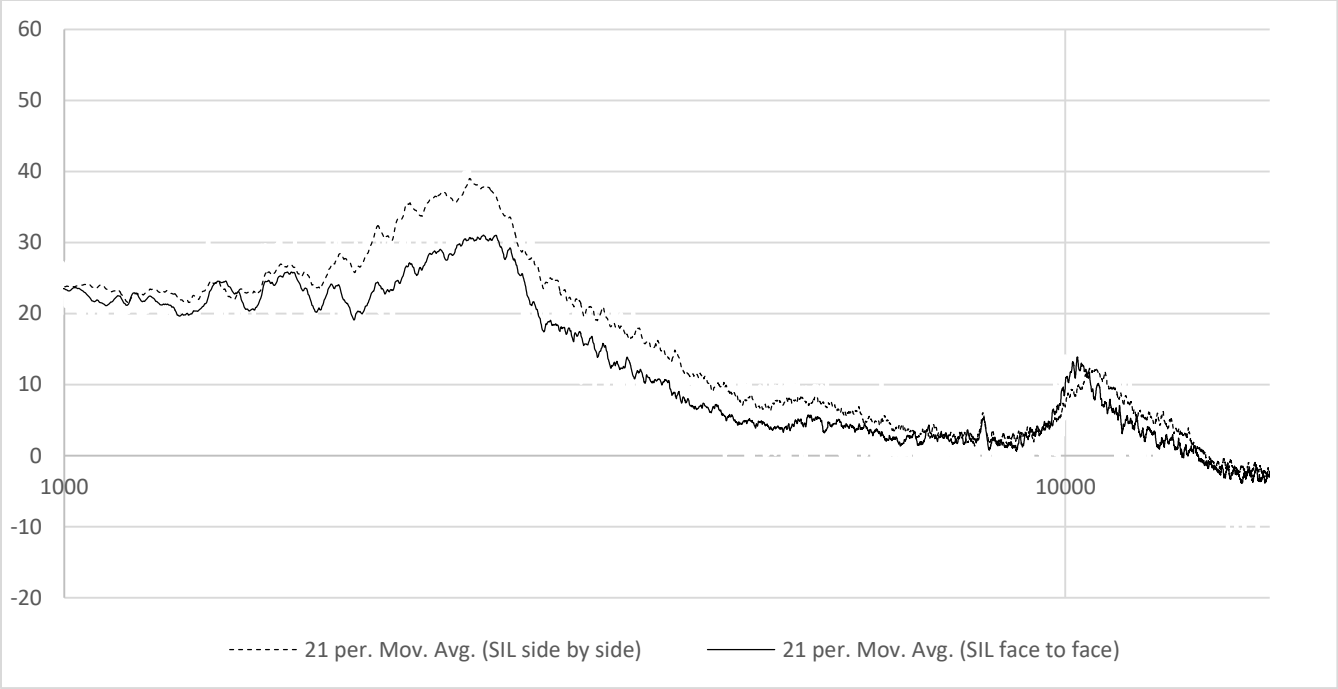

Figure 61: Sound intensity levels for the two-microphone configurations.

This comparison shows that the two configurations give similar measurements. The magnitude is different at low frequency, however, the side-by-side configuration is most likely less accurate.